Self-organization mechanisms for the formation of nearshore crescentic and transverse sand bars

M. CABALLERIA, G. COCO, A. FALQUÉS and D. A. HUNTLEY

Journal of Fluid Mechanics / Volume 465 / August 2002, pp 379 - 410
DOI: 10.1017/S002211200200112X, Published online: 02 September 2002

J. Fluid Mech. (2002), *vol.* 465, *pp.* 379–410.
DOI: 10.1017/S002211200200112X Printed in the United Kingdom

Self-organization mechanisms for the formation of nearshore crescentic and transverse sand bars

By M. CABALLERIA[1], G. COCO[2], A. FALQUÉS[3] AND D. A. HUNTLEY[4]

[1]Departament de Física i Matemàtica Aplicades, Universitat de Vic, 08500 Vic, Spain

[2]Complex Systems Laboratory, Scripps Institution of Oceanography, University of California San Diego, La Jolla, CA 92093-0225, USA

[3]Departament de Física Aplicada, Universitat Politècnica de Catalunya, 08034 Barcelona, Spain

[4]Institute of Marine Studies, University of Plymouth, Plymouth, PL4 8AA, UK

(Received 4 December 2000 and in revised form 22 November 2001)

The formation and development of transverse and crescentic sand bars in the coastal marine environment has been investigated by means of a nonlinear numerical model based on the shallow-water equations and on a simplified sediment transport parameterization. By assuming normally approaching waves and a saturated surf zone, rhythmic patterns develop from a planar slope where random perturbations of small amplitude have been superimposed. Two types of bedforms appear: one is a crescentic bar pattern centred around the breakpoint and the other, herein modelled for the first time, is a transverse bar pattern. The feedback mechanism related to the formation and development of the patterns can be explained by coupling the water and sediment conservation equations. Basically, the waves stir up the sediment and keep it in suspension with a certain cross-shore distribution of depth-averaged concentration. Then, a current flowing with (against) the gradient of sediment concentration produces erosion (deposition). It is shown that inside the surf zone, these currents may occur due to the wave refraction and to the redistribution of wave breaking produced by the growing bedforms. Numerical simulations have been performed in order to understand the sensitivity of the pattern formation to the parameterization and to relate the hydro-morphodynamic input conditions to which of the patterns develops. It is suggested that crescentic bar growth would be favoured by high-energy conditions and fine sediment while transverse bars would grow for milder waves and coarser sediment. In intermediate conditions mixed patterns may occur.

1. Introduction

Physical processes characterizing the nearshore region are still not clearly understood. As a consequence, the morphological changes leading to the observed variety of shapes and features appearing at different time and space scales is nearly impossible to predict. Sometimes the sea bed in the nearshore region is characterized by rhythmic longshore patterns of impressive regularity. Such patterns are usually detected only in restricted portions of the nearshore region. The most familiar example for the observer is probably given by beach cusps whose appearance is limited to the swash region (Russell & Mcintire 1965) and whose presence distinctly characterizes the shape of the coastline. Rhythmic features also appear and extend through the

surf zone, the most common example being the presence of megacusps (Short 1999) and transverse bars (Niederoda & Tanner 1970; Konicki & Holman 2000). Rhythmic patterns, usually called by the term 'crescentic bars', can also appear and be limited to the region around which waves break (Lippmann & Holman 1990). In some cases even a mixed topography with the concurrent presence of different types of these features has been reported (Davis & Fox 1972; Goldsmith, Bowman & Kiley 1982; Short 1999).

The formation of these rhythmic patterns has usually been related to the presence of regular structures in the hydrodynamics. Coupling between incoming waves and standing edge waves provides an alongshore structure affecting the sea bed morphology and resulting in the pattern formation. Such a mechanism has been proposed in order to explain the formation of beach cusps (Inman & Guza 1982), and crescentic and oblique bars (Bowen & Inman 1971; Holman & Bowen 1982). This approach, although successful in the prediction of the shapes and even initial alongshore spacing of the features, has failed more rigorous field testing (Holland & Holman 1996; Masselink & Pattiaratchi 1998) and, more generally, the hypothesis that sediment is just a reflection of the hydrodynamics without any feedback between flow and morphology seems inappropriate.

In fact, some recently developed models based on cellular automata (Coco, Huntley & O'Hare 2000; Werner & Fink 1993) show that the dynamical behaviour related to the formation and development of rhythmic patterns in the nearshore region is essentially the result of non-linear interactions between flow and morphology. Another approach commonly adopted to study the initial growth of a pattern is linear stability analysis which has already been successfully applied to describe the formation of various features at different scales ranging from ripples (Blondeaux 1990) to offshore patterns like sand waves (Hulscher, De Swart & De Vriend 1993) and shoreface-connected ridges (Calvete *et al.* 2001).

Linear stability analysis has also been considered for the formation of patterns characterized by length scales comparable to that of the nearshore region (Christensen, Deigaard & Fredsoe 1995; Deigaard *et al.* 1999; Falqués, Montoto & Iranzo 1996; Hino 1975; Vittori, De Swart & Blondeaux 1999). In particular, Falqués, Coco & Huntley (2000) have examined the coupling between sea bed disturbances and wave-driven water motion in the surf zone. Their analysis clearly indicated that sea bed disturbances can cause excess gradients in the radiation stresses leading to the growth of patterns around the breaking area resembling crescentic bars. Their investigation was carried out considering a monochromatic normally incident wave field and included the effect of a moving breaker line on the growth of the features. However, the refraction of the waves over the developing topography was not included and, of course, the linearity of the stability analysis allowed only for the small-amplitude behaviour of the features.

The study described here extends this work in two respects: (i) the assumption of linearity is relaxed and (ii) wave refraction is accounted for. To this end, a nonlinear model based on the shallow water equations capable of simulating the formation and finite-amplitude development of rhythmic patterns is presented, and the resulting features are shown and interpreted.

The next section is dedicated to the theoretical foundation and to the parameterizations of the model used for the simulation of rhythmic pattern formation and development, while in § 3 an outline of the numerical algorithm is given. Section 4 shows results obtained from numerical simulations including a sensitivity analysis of the significant parameters involved in the process and qualitative comparisons with

field observations. Section 5 is devoted to the interpretation of the physical mechanism for the growth of the features. Findings and limitations are discussed in §§ 6 and 7.

2. Formulation

2.1. *Averaged governing equations*

We consider a rectilinear coast with a shoreline given by the y-axis and with a topography described by the level of the sea bed, $z = z_b(x, y, t)$, where x is the cross-shore coordinate, positive in the offshore direction, and z is the vertical coordinate, positive upward ($z = 0$ corresponds to the mean water level). The morphological evolution is described by the sediment conservation equation

$$\frac{\partial z_b}{\partial t} + q_{j,j} = 0, \tag{2.1}$$

where $\boldsymbol{q}$ is the horizontal sediment flux vector (volume of sand per horizontal length unit and time unit). The horizontal coordinates will be hereinafter represented by $x_1 = x$, $x_2 = y$, and repeated indexes are assumed to be summed. The derivative with respect to x_j is indicated by the subindex j. The rate of change of sediment concentration above the bed has been neglected in (2.1) by assuming that the time scale of the changes in sediment concentration are much larger than the hydrodynamic time scale (see Appendix A). The correction due to sand porosity (factor ~ 0.5 in front of $\partial z_b/\partial t$) is omitted for simplicity and it is assumed to be included in the parameterization of the sediment flux.

The sediment flux is obviously related to water motion so that morphodynamic evolution requires knowledge of the hydrodynamics. The parameterization that will be used for sediment transport is based on the net mean current, depth and wave averaged, $\boldsymbol{v} = (v_1, v_2)$, so that the hydrodynamic equations will be the depth and wave-averaged momentum and mass conservation (Mei 1989)

$$\frac{\partial v_i}{\partial t} + v_j v_{i,j} = -g z_{s,i} - \frac{1}{\rho D}(\tau_i + S_{ij,j}) + \frac{1}{D}[\nu D(v_{i,j} + v_{j,i})]_{,j}, \quad i = 1, 2, \tag{2.2}$$

and

$$\frac{\partial D}{\partial t} + (D v_j)_{,j} = 0. \tag{2.3}$$

In these equations $D = z_s - z_b$ is the total depth and $z_s(x, y, t)$ stands for the free-surface elevation. The bottom shear stress is $\boldsymbol{\tau}$, and the water density is ρ. The fast water motions related to the turbulence and to the wind and swell waves are not explicitly described in the model. Their effects are parameterized through the Reynolds stresses (last right-hand-side term in (2.2)) with the turbulent momentum mixing coefficient ν (eddy viscosity) and the wave radiation stresses S_{ij}.

In principle, the shallow-water approximation is appropriate as long as interest is focused on morphological evolution at horizontal length scales of the order of the surf zone width, i.e. $O(10^2\,\mathrm{m})$, in water depths of $O(1\,\mathrm{m})$. The wave averaging is also sensible because the aim is the slow morphological evolution (time scales of hours) coupled to the net currents. Nevertheless, the vertical structure of the flow in combination with a non-uniform suspended sediment distribution in the water column can give an important contribution on the sediment flux. Also, because of the nonlinearity of the sediment transport, there can be a net transport due to the wave oscillatory motion even in the absence of a net current. The possibility of either

disregarding these effects or their parameterization into the shallow water model will be discussed in § 2.2 and in Appendix B.

After introducing the pertinent parameterizations, equations (2.1), (2.2) and (2.3) constitute a system of four nonlinear partial differential equations for the four unknowns $z_b(x, y, t)$, $\boldsymbol{v}(x, y, t)$ and $z_s(x, y, t)$.

2.2. *Parameterizations*

2.2.1. *Incident waves*

The aim of this paper is to show that the mean water motions, driven by the wind or swell waves incoming from deep water and coupled to the topographic evolution, can generate morphological patterns like crescentic and transverse bars. The wave forcing on the mean hydrodynamics is given by the radiation stress

$$S_{ij} = E\left[\left(\frac{c_g}{c} - \frac{1}{2}\right)\delta_{ij} + \frac{c_g}{c}\frac{k_i}{k}\frac{k_j}{k}\right], \quad i = 1, 2, \tag{2.4}$$

where $\boldsymbol{k}$ and E are the wavenumber and the energy density of the waves, respectively, and c, c_g are their phase and group celerities (Horikawa 1988). All these quantities are assumed to be known in deep water. However, as the waves approach the coast they refract, the energy density slightly increases (shoaling) and then decreases drastically due to breaking in the surf zone. The phase and group celerities change because of the reduction in water depth and the modification of the wavenumber. Wave transformation will be described here in a simplified way that includes only the essential physical processes. The drastic reduction in wave energy as waves break, coupled to the topographic irregularities, has proven to be a possible cause of the initial formation of crescentic bars (Falqués *et al.* 2000). On the other hand, early studies by Niederoda & Tanner (1970) and many field observations (see for instance Falqués 1989) suggest that wave refraction can be very important for transverse bar formation. Thus, we will try to incorporate these two effects into the model and to leave out unnecessary complications. To this end, regular waves will be assumed, i.e. all the individual waves have the same amplitude and wavenumber at a given location. Moreover, infragravity wave motions are disregarded in this study.

The wave energy density distribution

$$E = \tfrac{1}{8}\rho g H^2 \tag{2.5}$$

is provided by the wave height H at each location. Wave height will be assumed to be proportional to the water depth

$$H = \gamma_b D \tag{2.6}$$

in the surf zone (saturated surf zone hypothesis) and constant out of the surf zone. As discussed in § 6, this last assumption is based on the fact that the increase in wave amplitude because of the shoaling is smaller than the reduction due to breaking in the surf zone. The same wave amplitude distribution was considered in Falqués *et al.* (2000). However, its implementation in the present nonlinear model is not straightforward. First, the position of the breaking line, $x = X_b(y, t)$, has to be determined. Given the deep-water wave height, H_∞, this is done by seeking the first location where $\gamma_b D(x, y, t) = H_\infty$ along each wave ray. Second, once waves start to break because of the depth reduction their amplitude decreases according to (2.6). If the depth reduction following the wave path is reversed (i.e. due to the presence of a bar) equation (2.6) predicts an onshore wave amplitude increase which is not

observed in nature. Therefore, the model does not allow the amplitude to grow in this case and instead, it takes a constant wave height along the ray, H_1, up to the position where the condition $H_1 = \gamma_b D(x, y, t)$ is met.

From the frequency of the incident waves, σ, the dispersion relation allows the computation of the magnitude of the wavenumber:

$$\sigma^2 = gk \tanh(kD). \tag{2.7}$$

The standard expressions from linear wave theory (Mei 1989; Horikawa 1988) provide the phase and group celerities.

Since infragravity oscillations are not considered in this study, the wave field has been assumed to be quasi-steady, i.e. changing only at the slow time scale of the topographic changes. Thus, the equation for a ray, $y = y(x)$,

$$\frac{\mathrm{d}}{\mathrm{d}x}\left[\frac{ky'}{\sqrt{1+y'^2}}\right] = \sqrt{1+y'^2}\frac{\partial k}{\partial y}, \tag{2.8}$$

can be derived by using the geometric optics approximation (Mei 1989, p. 65). If we consider a given location (x_0, y_0) and a new Cartesian coordinate system with its origin at (x_0, y_0), and with axes x^* and y^* parallel and perpendicular respectively to ∇D, then y^* is parallel to the local depth contour and $\partial k/\partial y^* = 0$. This allows equation (2.8) to be rewritten as the Snell law

$$\frac{\mathrm{d}}{\mathrm{d}x^*}(k \sin\varphi^*) = 0, \tag{2.9}$$

where φ^* is the angle between the wave ray and the x^*-axis, that is, the normal to the perturbed depth contours.

2.2.2. *Sediment transport*

The net (wave-averaged) sediment transport in the surf zone is jointly driven by currents and by waves, the latter contributing because, as it is a nonlinear process, there is also a net effect from the wave oscillatory motion. Transport takes place both in suspension (suspended load) and in contact with the bed (bed load) and it is a complicated process which is still poorly understood and hard to predict accurately. However, it is usually accepted (see Horikawa 1988, for instance) that the processes associated with *cross-shore transport* and *longshore transport* are different. The longshore transport is dominated by the effect of the longshore current which typically has a simple vertical profile characteristic of a steady unidirectional flow. On the other hand, any attempt to understand and predict the cross-shore transport needs to deal necessarily with a more complicated vertical structure of the flow and with the complexity of the wave oscillatory motion (Battjes 1988; van Rijn 1993).

However, the cross-shore sediment transport vanishes for the alongshore uniform and steady equilibrium. In this situation, for normal wave incidence there is no net flux of water, $\boldsymbol{v} = 0$, the onshore wave transport being compensated by the wave-induced baroclinic current (e.g. undertow). Also the net sediment transport vanishes, $\boldsymbol{q} = 0$, as a result of a balance between the onshore-wave-driven sediment transport (by wave asymmetry, for instance) and the offshore transport due to gravity and undertow. If alongshore gradients in the topography develop, alongshore gradients in wave radiation stresses and, thereby, gradients in set-up arise. In this way, a horizontal circulation (with possibly rip currents) with a non-vanishing depth-averaged flow, $\boldsymbol{v} \neq 0$, is generated. This type of circulation is commonly observed in the field where

crescentic bars or transverse bars are present, and it is known to carry a significant amount of sediment, typically larger than unperturbed (longshore uniform) cross-shore transport (Short 1999). The key assumption that has been tested in the present study is that, even if other effects can have some influence, the main mechanism responsible for the formation of the bars is the coupling between the morphology and the circulation via the sediment transport driven only by the depth-averaged current. Therefore, we assume that the departure of sediment transport from equilibrium depends on the departure on depth-averaged current. Keeping this in mind a sediment transport parameterization given by

$$\boldsymbol{q} = \alpha(u_0)\boldsymbol{v} - \gamma(u_0)\nabla h \tag{2.10}$$

is assumed, where $h(x, y, t) = z_b(x, y, t) - z_b^0(x)$ is the topographic perturbation with respect to equilibrium and u_0 is the wave orbital velocity at the bed. The linearity of the dependence with respect to the current is realistic when the current is small with respect to the wave orbital velocity, $|\boldsymbol{v}| \ll u_0$. However, as argued when analysing the physical mechanism underlying the growth of the bars (§ 5), that assumption is not essential. More details on the choice of this parameterization and, in particular, the reason for the term in ∇h, are given in Appendix B.

The structure of the α and γ functions is taken from Falqués *et al.* (2000) since one of the main interests of the present paper is to extend the linear stability analysis presented there. The particular choices can be supported by at least two different approaches. First, the Bailard (1981) energetic formulation for suspended load transport and weak current, $|\boldsymbol{v}| \ll u_0$, has this form with

$$\alpha(u_0) = C_1 u_0^3, \quad \gamma(u_0) = C_1 \varepsilon_s \frac{u_0^5}{w}, \tag{2.11}$$

where $C_1 = \varepsilon_s c_d/(gw)$, w represents the sediment fall velocity and ε_s is a non-dimensional constant of order 10^{-2}. A similar expression holds for bedload with α and γ proportional to u_0^2 and u_0^3, respectively. Alternatively, $\alpha\boldsymbol{v}$ can be seen as the transport in suspension in the case of a vertically uniform sediment concentration, α/D (a well-mixed water column because of turbulence, see, for instance Peters & Dette 1999). The coefficient γ can then be introduced as an heuristic way of taking into account morphological diffusion. Clearly, the second right-hand-side term in (2.10) leads to a diffusive term when the expression for $\boldsymbol{q}$ is introduced in the morphodynamic equation (2.1). Independently of the formulation, (2.10) means that the sediment is stirred by the waves and advected by the current. Thus, the α function will be referred to as the *wave stirring function.*

In the alongshore uniform equilibrium, the orbital velocity is a known function of the cross-shore coordinate, $u_0 = u_0(x)$. Out of equilibrium, the perturbed orbital velocity depends also on the alongshore coordinate in response to the alongshore gradients in wave energy. For the linear stability analysis presented in Falqués *et al.* (2000) the perturbation in u_0 produced a second-order correction in $\alpha(u_0)\boldsymbol{v}$ since $\boldsymbol{v}$ was first order. Therefore, this perturbation was neglected and the wave stirring was assumed to be a fixed known function of the cross-shore coordinate, $\alpha(x)$. Several choices for this function were tested and the conclusion was that the growth of morphological instabilities required only that $\alpha(x)$ increased faster than $D(x)$ through the surf zone and was constant or decaying outside the surf zone. From a physical point of view it is likely to be true for suspended load since either (i) α is proportional to a power three of the wave orbital velocity which is proportional in turn to the water depth to power 1/2 or (ii) α/D is the sediment concentration which should

increase seaward as the wave-induced bed shear stress increases. This is consistent with field observations by Antsyferov & Kos'yan (1990, figure 12) or by Peters & Dette (1999, figures 8 and 9) where it is shown how the concentrations of suspended sediment tend to increase seaward across the surf zone and then diminish offshore of the breaking zone. As shown in Falqués *et al.* (2000), such a distribution of suspended sediment can only be expected if infragravity contributions are limited, otherwise the stirring function should be approximately constant across the surf zone.

For simplicity, the same unperturbed structure of the α function has been used for the finite-amplitude simulation. As will be seen through the analysis of the instability mechanism in § 5, the possible alongshore gradients in $\alpha(x, y)$ are not essential for the mechanism itself. Additional tests allowing for such gradients have been run. In such tests, the structure of the α function depended on the local water depth (and so on the bed perturbation) rather than the cross-shore position. Nevertheless, simulations still resulted in the growth of rhythmic patterns characterized by the same finite amplitude, configuration and growth rate as the runs with the simplified structure of the α function.

Since the essential condition for the growth of bedform is that $\alpha(x)/D(x)$ is an increasing function in the surf zone and since $D(x)$ is linear, $\alpha(x)$ was chosen to be quadratic up to the breaking point and smoothly decaying beyond. The magnitude of α will be represented by its maximum, $\alpha_m = \{\alpha(x)\}_{\max}$. Similarly, the morphological diffusion $\gamma(x)$ has been assumed to increase up to the breaking line and decrease beyond. Its maximum value, $\gamma_m = \{\gamma(x)\}_{\max}$, is another important parameter of the model. Simulations have been run changing the free parameters shaping $\alpha(x)$ and $\gamma(x)$ but the results do not change significantly (in agreement with the results of the linear stability analysis by Falqués *et al.* 2000).

2.2.3. *Turbulent momentum diffusion*

Wave breaking dissipates wave energy into turbulent water motions. It is commonly accepted that these turbulent motions include small-scale horizontal eddies that produce a horizontal momentum diffusion represented by the Reynolds stresses in (2.2) which are proportional to the eddy viscosity coefficient ν that depends in turn on the wave energy dissipation rate. A very simple formulation based on Longuet-Higgins (1970) will be used here. Accordingly, the kinematic eddy viscosity will be taken as

$$\nu = Nx\sqrt{gD}, \tag{2.12}$$

where N is a non-dimensional parameter. However, since the maximum turbulence occurs close to the breaking line and beyond the breaking line a decrease of the turbulence is expected, an exponential decay is assumed seaward of the breaking line (with results being unaffected by the specific rate of decay). This formulation is mathematically consistent with Battjes (1975) for a wave energy dissipation rate of $\mathscr{D} = \rho(gD)^{3/2}$.

2.2.4. *Bed shear stress*

The instantaneous bed shear stress is proportional to the square of the total flow velocity at the bottom boundary layer with a certain drag coefficient. If a proportionality is assumed between the bed flow velocity and the depth-averaged velocity, there is a similar dependence between the shear stress and the depth-averaged velocity but with a corrected drag coefficient, c_d. The momentum equations

(2.2) are wave averaged and therefore the averaged-bed shear stress

$$\boldsymbol{\tau} = -\rho c_d \langle |\boldsymbol{v} + \boldsymbol{v}'| (\boldsymbol{v} + \boldsymbol{v}') \rangle, \tag{2.13}$$

is needed, where $\langle \cdot \rangle$ means time average over the wave period and $\boldsymbol{v}'$ is the wave velocity component, with amplitude u_0. Since the interest in this paper is on normal wave incidence, the currents will not be very strong and the weak current limit, $|\boldsymbol{v}| \ll u_0$, will be assumed. Thus, the averaged bottom shear stress (2.13) will be approximated by

$$\tau_x = -\frac{2}{\pi} \rho c_d u_0 \, [v_x (1 + \cos^2 \varphi) + v_y \sin \varphi \cos \varphi], \tag{2.14}$$

$$\tau_y = -\frac{2}{\pi} \rho c_d u_0 \, [v_x \sin \varphi \cos \varphi + v_y (1 + \sin^2 \varphi)], \tag{2.15}$$

where φ is the wave incidence angle with respect to the $-x$-direction, i.e. $k_x = -k \cos \varphi$, $k_y = k \sin \varphi$ (Horikawa 1988, p. 120). Note that $\varphi = 0$ in deep water but $\varphi \neq 0$ in the surf zone as the waves are refracted by the emerging bars.

3. Nonlinear numerical model

The governing equations (2.1), (2.2) and (2.3) have been solved numerically to give the time evolution of the topography and the mean hydrodynamics under the forcing of incident waves from any permutation of random perturbations to a planar beach. As shown in the following sections, the numerical model (called *morfo50*) describes the formation and further evolution of crescentic and transverse bars from small initial topographic irregularities.

3.1. *Geometry and boundary conditions*

A rectilinear coastline given by the y-axis is assumed with an alongshore uniform reference beach profile which consists of a small vertical wall at the shoreline, then a linear slope, a transition topography defined by a second-order polynomial and, finally, a horizontal bottom:

$$z_b^0(x) = \begin{cases} z_0 + \beta x, & 0 \leqslant x \leqslant x_1 \\ z_\infty - \dfrac{\beta}{2} \dfrac{(x - x_2)^2}{x_2 - x_1}, & x_1 \leqslant x \leqslant x_2 \\ z_\infty, & x_2 \leqslant x. \end{cases} \tag{3.1}$$

This beach profile will be assumed to be in equilibrium, in the sense that the wave-driven sediment transport is balanced by the downslope gravitational transport according to (B 5). Even though this simplified profile does not correspond exactly with any of the equilibrium profiles found in field observations or used in modelling (Dean 1991; Plant, Ruessink & Wijnberg 2000), it shares with them the main qualitative characteristic which is its concavity. In view of the fact that the investigation of equilibrium beach profiles is still under way (Plant *et al.* 2000) and that we are interested in alongshore non-uniform features, this seems a reasonable choice. The vertical wall at the shoreline is introduced in order to avoid the complications of a moving shoreline and the dynamics of the swash zone that are expected to have little effect on the surf zone bars.

To investigate the formation and dynamics of nearshore patterns we will consider a rectangular horizontal domain bounded by the shoreline, $x = 0$, an offshore boundary,

$x = L_x$, and two cross-shore straight lines, $y = 0$, $y = L_y$. The offshore boundary will be chosen in order that the surf zone fits well into the domain, i.e. at least at a distance of twice the width of the surf zone. Since we are interested in bar systems which are rhythmic along the coast, periodic boundary conditions will be assumed at the lateral sides of the domain:

$$z_b(x,0,t) = z_b(x,L_y,t), \quad z_s(x,0,t) = z_s(x,L_y,t), \quad \boldsymbol{v}(x,0,t) = \boldsymbol{v}(x,L_y,t). \tag{3.2}$$

Of course, the results of the model have to be carefully checked for sensitivity to the length of the domain L_y. To be consistent with our crude representation of the swash zone, no sediment will be allowed to move onshore or offshore at the shoreline:

$$q_x(0,y,t) = 0, \tag{3.3}$$

and, in addition, the non-slip condition of viscous flows

$$\boldsymbol{v}(0,y,t) = 0 \tag{3.4}$$

will be assumed. In the reference state without bars there is no circulation since the wave angle of incidence is perpendicular to the coast. When the bars develop, a circulation coupled to them also develops. Since the topographic patterns are located in the nearshore region, flow patterns will be expected to develop in such an area as well with the flow velocities vanishing far offshore. Consequently, the following boundary conditions will be considered:

$$\kappa_x \frac{\partial v_x}{\partial x} + v_x = 0, \quad \kappa_y \frac{\partial v_y}{\partial x} + v_y = 0, \quad x = L_x, \tag{3.5}$$

with the constant coefficients κ_x, $\kappa_y > 0$ forcing an exponential seaward decay across the offshore boundary.

3.2. *Spatial discretization*

Spatial discretization has been achieved by using finite differences with a grid spacing

$$\Delta x = \frac{L_x}{N_x - 1}, \quad \Delta y = \frac{L_y}{N_y}.$$

A staggered grid scheme has been used where the scalar variables such as the free surface and the bottom levels, z_s, z_b, the wave height H, the incident wave angle φ, etc. are defined at the centre of each cell, which will be referred as the η-node:

$$x_i = (i - \tfrac{1}{2})\Delta x, \quad i = 1,\ldots,N_x, \quad y_j = (j - \tfrac{1}{2})\Delta y, \quad j = 0,\ldots,N_y + 1.$$

The vector variables such as the velocity $\boldsymbol{v}$ and the sediment flux $\boldsymbol{q}$ are defined at the boundaries of each cell. Thus, the cross-shore components are defined at the so-called u-nodes:

$$x_i = (i-1)\Delta x, \quad i = 1,\ldots,N_x, \quad y_j = (j - \tfrac{1}{2})\Delta y, \quad j = 0,\ldots,N_y + 1,$$

and the longshore components at the v-nodes:

$$x_i = (i - \tfrac{1}{2})\Delta x, \quad i = 1,\ldots,N_x, \quad y_j = (j-1)\Delta y, \quad j = 0,\ldots,N_y + 1.$$

The derivatives are evaluated by central second-order-difference approximations. An example is given in § 3.4.

3.3. *Wave refraction in finite difference form*

In order to evaluate the wave radiation stress, the incidence angle φ with respect to the $-x$-direction must be determined. The discretized stepwise bottom leads, through the dispersion relation (2.7), to a discrete set of values for the magnitude of the wavenumber, $k_{i,j}$, over the whole domain. Therefore, a ray crossing from one cell to the next will feel a jump in the wavenumber and, according to the local Snell law (2.9), a jump in the local incidence angle φ^* given by

$$k_{i,j} \sin \varphi^*_{i,j} = k_{i-1,j} \sin \varphi^*_{i-1,j} \tag{3.6}$$

will occur. The incidence angle with respect to the cross-shore direction is given by $\varphi_{i,j} = \varphi^*_{i,j} + \theta_{u\,i,j}$ where $\theta_{u\,i,j}$ is the angle between the normal to the local depth contour, $(\nabla D)_{u\,i,j}$, and the x-axis, evaluated at the u-node i, j.

The present formulation has two limitations. First, the Snell law is applied by progressing along each cross-shore line (decreasing i, fixed j) instead of keeping track of the wave rays (a similar procedure is also used to control the wave amplitude decrease in the shoreward direction). This is appropriate as long as the incidence angle φ is not too big. Furthermore, whenever waves propagate from deep to shallow water, the wavenumber increases along the ray path, $k_{i-1,j} > k_{i,j}$, and (3.6) allows the computation of $\varphi^*_{i-1,j}$ from $\varphi^*_{i,j}$. However, in the presence of shoals and pools, waves can propagate from shallow to deep water with the result that

$$\frac{k_{i,j}}{k_{i-1,j}} \sin \varphi^*_{i,j} > 1 \tag{3.7}$$

may occur and $\varphi^*_{i-1,j}$ is no longer defined. In physical terms this means that wave reflection occurs and has the consequence that, for incidence angles above a critical angle, the simple wave refraction formulation is not allowed. This happens for bedforms of large amplitude and, as will be seen, it poses the most severe limitation on the model simulations. However, the critical bar amplitudes are relatively high so that the model is capable of describing the formation and further evolution of sand bars up to amplitudes (from trough to crest) of a few decimetres.

3.4. *Time stepping*

The variables are defined at the time mesh

$$t_n = n\Delta t, \quad n = 0, \ldots, N_t,$$

and the temporal integration is by a second-order Adams–Bashforth scheme that approximates $\mathrm{d}s/\mathrm{d}t = \phi(s,t)$ by

$$\frac{s^n - s^{n-1}}{\Delta t} = \tfrac{3}{2}\,\phi^{n-1} - \tfrac{1}{2}\,\phi^{n-2}, \tag{3.8}$$

where $s^n = s(t_n)$. The initial time step from $n = 0$ to $n = 1$ is performed by an explicit Euler scheme.

The combination of the spatial and the temporal discretization yields the difference form of the governing equations (2.1), (2.2), (2.3), from where $z_b, z_s, \boldsymbol{v}$ can be computed at $t = n\Delta t$ from their values at $t = (n-1)\Delta t$ and $t = (n-2)\Delta t$. For instance, the mass

conservation equation (2.3) becomes

$$\begin{aligned}\frac{D_{i,j}^{n}-D_{i,j}^{n-1}}{\Delta t} = &-\frac{3}{2}\frac{1}{\Delta x}(D_{u\,i+1,j}^{n-1}u_{i+1,j}^{n-1}-D_{u\,i,j}^{n-1}u_{i,j}^{n-1})\\ &-\frac{3}{2}\frac{1}{\Delta y}(D_{v\,i,j+1}^{n-1}v_{i,j+1}^{n-1}-D_{v\,i,j}^{n-1}v_{i,j}^{n-1})\\ &+\frac{1}{2}\frac{1}{\Delta x}(D_{u\,i+1,j}^{n-2}u_{i+1,j}^{n-2}-D_{u\,i,j}^{n-2}u_{i,j}^{n-2})\\ &+\frac{1}{2}\frac{1}{\Delta y}(D_{v\,i,j+1}^{n-2}v_{i,j+1}^{n-2}-D_{v\,i,j}^{n-2}v_{i,j}^{n-2}),\end{aligned}$$

where $D = z_s - z_b$ and $D_{u\,i,j} = (D_{i,j} + D_{i-1,j})/2$ and $D_{v\,i,j} = (D_{i,j} + D_{i,j-1})/2$ are the interpolated values of D at the u- and v-nodes, respectively. Similar cumbersome expressions hold for the rest of the governing equations.

Since the temporal integration is achieved by an explicit scheme, two generic stability conditions are expected:

$$\Delta t \leqslant c_1\frac{\min\{\Delta x^2, \Delta y^2\}}{\nu_{\max}}, \quad \Delta t \leqslant c_2\frac{\min\{\Delta x, \Delta y\}}{c_{\max}}, \tag{3.9}$$

the first one related to the parabolic nature of the system, the second one to its hyperbolic character. Given the values of the grid spacing, the momentum diffusivity and the shallow-water wave celerity, $c = \sqrt{gD}$, the latter inequality has proven to be the most restrictive in the numerical experiments, with a constant $c_2 \simeq 0.1$.

4. Model results

4.1. *Model sensitivity*

The numerical code presented in the previous section has been used to simulate the development of the sea bed in the nearshore region and the resulting formation of rhythmic patterns. Initial tests have been entirely devoted to the analysis of the model sensitivity and stability in relation to numerical parameters like the number of discretization points for a given domain. It has been found that the formation of the morphological patterns is not the result of a numerical instability, and changes, reduction or increase, in the number of discretization points only affects the definition of the features. Simulations described in this paper are all derived using at least a node every 1.5 m with results not being sensitive to doubling or halving this value. The previously described geometry of the beach profile involves the use of a small vertical wall at the shoreline (§ 3.1) whose height has been kept equal to 0.2 m for all the simulations presented in this paper. Because of the use of periodic boundary conditions, an important aspect to be carefully addressed concerns the width of the domain in the alongshore direction. The use of small domains could potentially cause two sources of error: a fast growth of what is only a spurious instability or the formation of patterns whose spacing does not lead to an equilibrium configuration. The first source of error has been categorically dismissed by comparing simulations with different widths of the domain and, in all the cases analysed, morphological patterns developed with the same flow pattern. The second source of error required particular care and domains were chosen in such a way that at least two wavelengths could fully develop. For the offshore boundary condition, values of $\kappa_x = \kappa_y = 30$ m were chosen in order to force a seaward decay towards zero (the rate of decay is e^{-1} in a distance

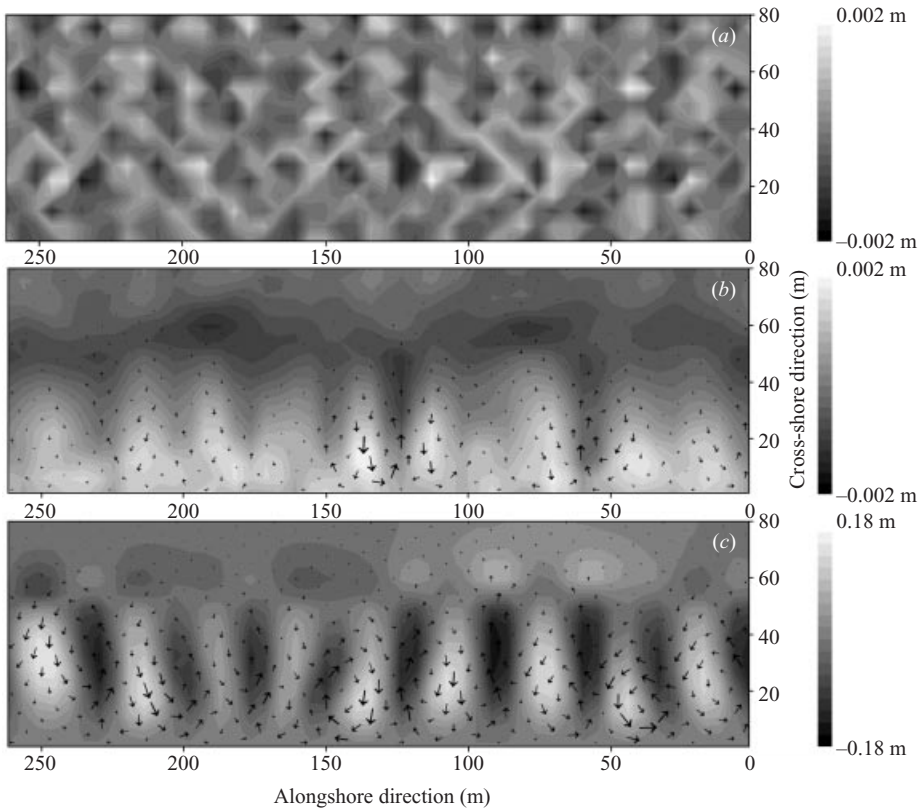

FIGURE 1. Formation and development of a transverse bar pattern. (*a*) Initial bed level perturbation, (*b*) bed perturbation after 1 h, and (*c*) final configuration reached after 5 h. Shoals and troughs are represented by light and dark colours respectively. Arrows represent the velocity field (maximum velocity in (*b*) $= 0.10\,\mathrm{m\,s^{-1}}$, maximum velocity in (*c*) $= 0.67\,\mathrm{m\,s^{-1}}$). The coastline is at the bottom of each plot.

of 30 m). We did not detect any significant change in the results by changing those values. In order to test the sensitivity of the model, simulations have been run under a variety of conditions for both the hydrodynamic and morphological parameters.

4.2. *Topography developmemt*

Simulations presented herein are all characterized by an initially planar slope with $\beta = 0.02$, a transition concave profile near $x = 120\,\mathrm{m}$ and a horizontal bottom according to the bathymetry introduced in § 3.1. As previously specified, the hydrodynamic conditions always refer to waves approaching normally to the coast. The deep-water wave height H_∞ is increased linearly with time from zero at $t = 0$ up to to its final value, and then kept constant through the rest of the simulation. This final value is achieved around $t_h = 20\,\mathrm{min}$. In all the simulations, the initial small perturbation is introduced only in the topography while the water is assumed to be initially at rest. Presumably, similar results would be obtained in the opposite case or in case of starting from perturbations in both the topography and the water.

For high values of morphological diffusivity, γ_m, the initial perturbation is washed out and the system goes back to the basic equilibrium topography. This is in accordance with the linear stability analysis presented in Falqués *et al.* (2000). Below some threshold in γ_m, the perturbation grows in time and large-scale rhythmic topography

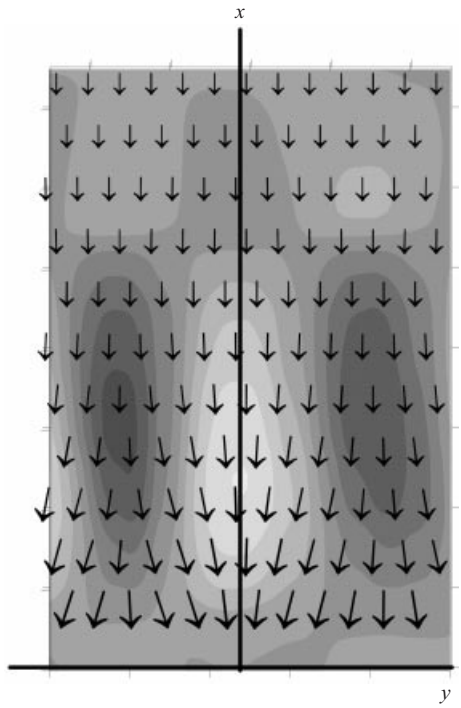

FIGURE 2. Topographic refraction of the incident waves by a transverse bar. The wavenumber field of the waves on the transverse bar (white) and the adjacent troughs (dark) is represented. The shoreline is at the bottom (y-axis).

develops. Even though quite complex patterns can form, the results show that the dynamics are governed by the competition between two basic configurations: crescentic bars (hereinafter CB) and transverse bars (TB), the former already predicted by the linear stability analysis of Falqués *et al.* (2000) while the latter is new. Depending on the model parameters pure CB or TB patterns or mixed topographies can occur. We first describe pure TB and CB growth and then report on the competition between these morphologies.

4.3. *Transverse bars*

Figure 1 shows different stages during the formation of a transverse bar pattern. It can be seen that there is a transition from a random topography (a) where no pattern can be detected into a trasverse one (b, c). Parameters considered in this simulation are: incident wave period $= 6$ s, $N = 0.005$, $\gamma_b = 0.8$, $H_\infty = 1$ m (as a result the breaking line is around 50 m), $c_d = 0.002$, $\gamma_m = 0.01\,\mathrm{m^2\,s^{-1}}$. In all the simulations, $\alpha_m = 0.01$ m has been chosen. The motivation for this choice will be discussed in § 6. The configuration after one hour is already very similar to the final one although some readjustments (see for example the area around 100 m in the alongshore direction) in the position and spacing of the features are evident.

The flow pattern related to the features is, as expected, with onshore flow over the crests of the bar while offshore flow can be observed in the troughs. This is consistent with the general property that a shoal (pool) in the surf zone tends to create an onshore (offshore) net flow because of the increase (decrease) in wave breaking. However, in the case of transverse bars there is another important effect

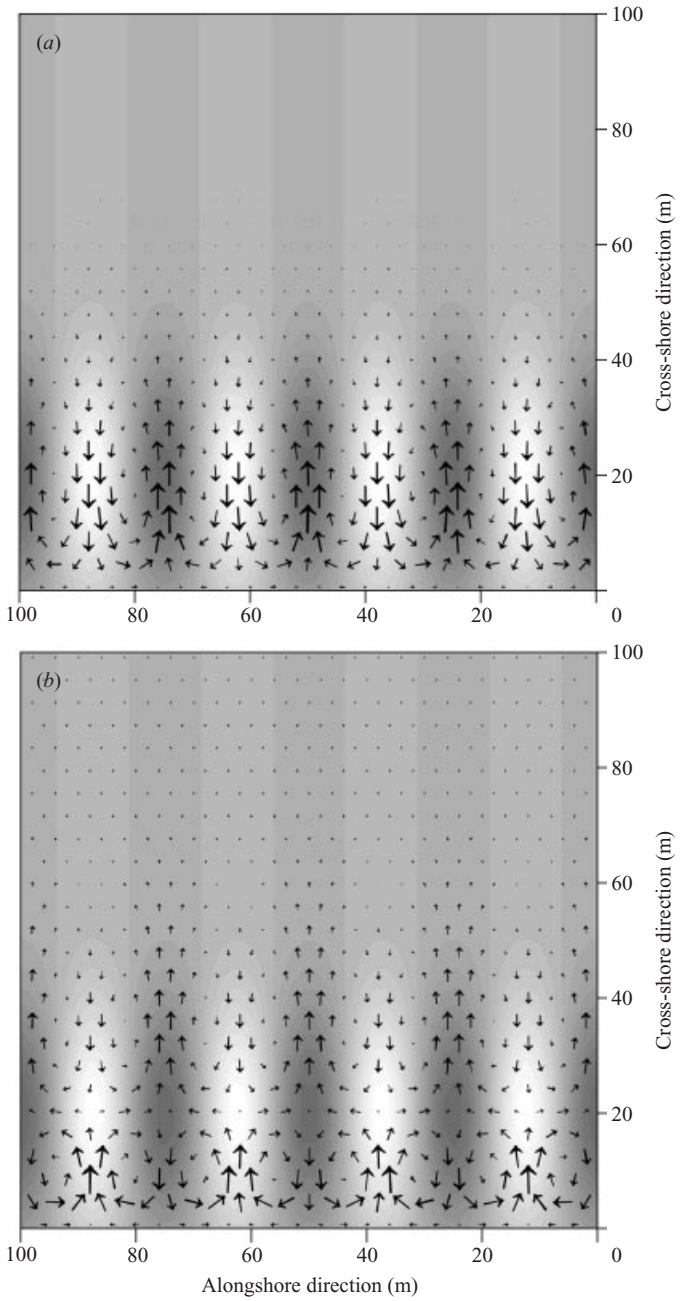

FIGURE 3. Flow pattern produced by artificial transverse bars either with wave refraction (*a*) or without wave refraction (*b*). Bar maximum relief 0.1 m, wave height $H = 1$ m. Shoals and troughs are represented by light and dark colours respectively. The maximum arrow in (*a*) corresponds to 0.5 m s^{-1} in (*a*) and to 0.09 m s^{-1} in (*b*), respectively. The coastline is at the bottom of each plot.

which reinforces the onshore flow at the crests. Because of the shallow depth over their crests, the bars produce a significant wave refraction so that the wave fronts slow down over the crests in comparison with the troughs (see figure 2). This 'focusing lens effect' on the incident waves is clearly visible by the casual observer whenever

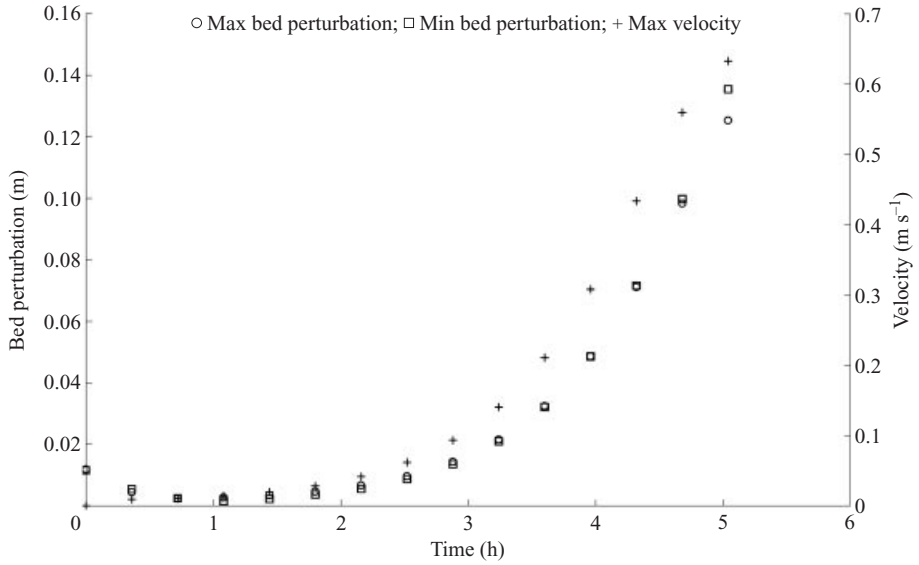

FIGURE 4. Growth of the maximum and minimum perturbation (absolute value) and of the maximum velocity for the simulation shown in figure 1.

transverse bars are present (see e.g. Falqués 1989). It produces a strong onshore current at the crests (up to 0.7 m s^{-1}) and was suggested by Niederoda & Tanner (1970) to be the main cause of transverse bar formation. Our simulations confirm the hypothesis of Niederoda & Tanner (1970): model runs which left out wave refraction did not result in the growth of transverse bars. As shown in figure 3, model runs without wave refraction and with artificially created transvers bars (through the initial topography) gave a much weaker circulation (not larger than 0.09 m s^{-1} for a bar relief of 0.1 m) with a somewhat different structure that explains why the bars do not grow in this case (see, for instance, the offshore directed current at the shore attachment). An interpretation of the importance of wave refraction for transverse bars will be given in § 5.3.

The growth of the features is also evident by analysing the growth rates of max/min amplitude and maximum velocity (figure 4). Maximum amplitude values for both the bed perturbation and the velocity field do not grow significantly during the first 3 hours. During this time interval, sediment is simply being organized into the transverse bar shape and only afterwards is a sharp growth in the amplitudes observed. The final amplitude of the features in the model is around 0.2 m, a value in reasonable agreement with the field observations (Niederoda & Tanner 1970; Konicki & Holman 2000). Nevertheless, such a comparison cannot be conclusive as, due to the previously indicated shortcomings in the way refraction is computed, the model does not reach a final steady equilibrium or even a state where a decay in the growth rates can be detected. The spacing of the features is around 30 m corresponding to around half the width of the surf zone. This latter value has been found to be stable and insensitive to changes in wave height or in the model parameterization but no rigorous comparison with field measurements could be made because of the lack of detailed data.

4.4. *Crescentic bar*

The formation and development of crescentic bars has also been successfully simulated by the present model and its sensitivity to the parameterization analysed in

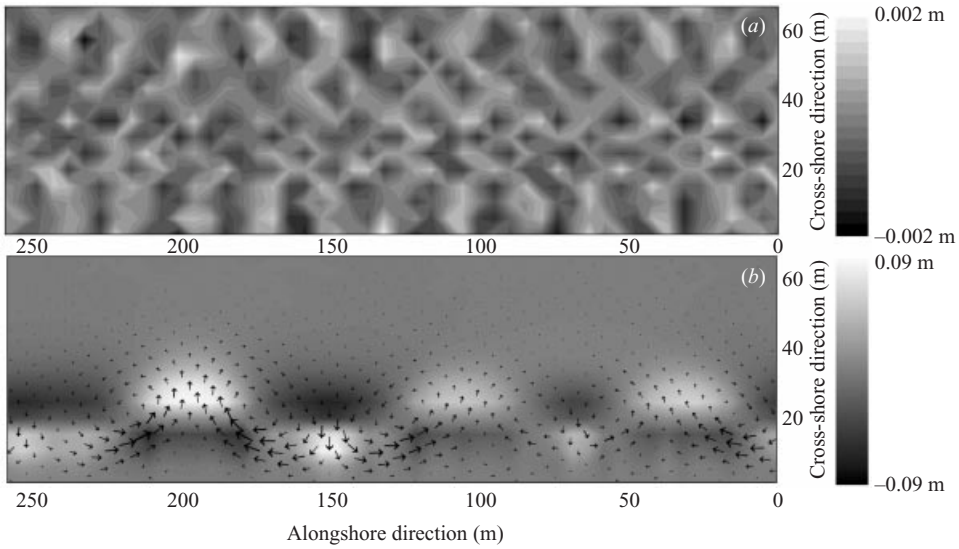

FIGURE 5. Formation and development of a crescentic bar pattern. (*a*) Initial bed level perturbation, and (*b*) final configuration reached after 3 h. Shoals and troughs are represented by light and dark colours respectively. Arrows represent the velocity field (maximum velocity in (*b*) = 0.38 m s^{-1}). The coastline is at the bottom of each plot.

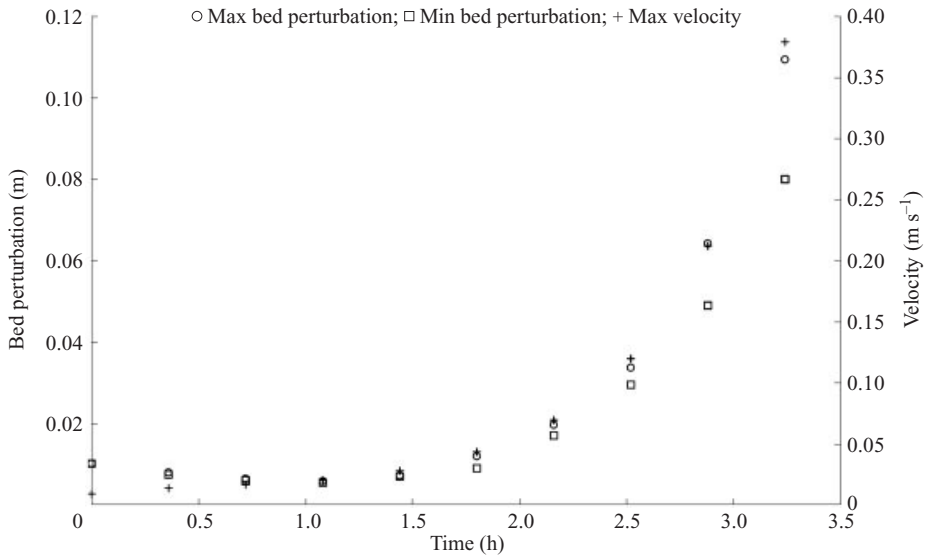

FIGURE 6. Growth of the maximum and minimum perturbation (absolute value) and of the maximum velocity for the simulation shown in figure 5.

detail. Figure 5 shows results obtained when running the model with the same parameterization previously considered apart from $H_\infty = 0.5$ m (breaking is around 25 m in the cross-shore direction). Figure 5(*a*) shows the initial, randomly generated, bed perturbation while figure 5(*b*) shows the final configurations reached after 3 h. The formation of a crescentic pattern with troughs and shoals alternating around the breaking line is evident. The flow pattern again presents onshore (offshore) flow over the shoals (troughs) inside the surf zone and vice versa outside the surf zone. The

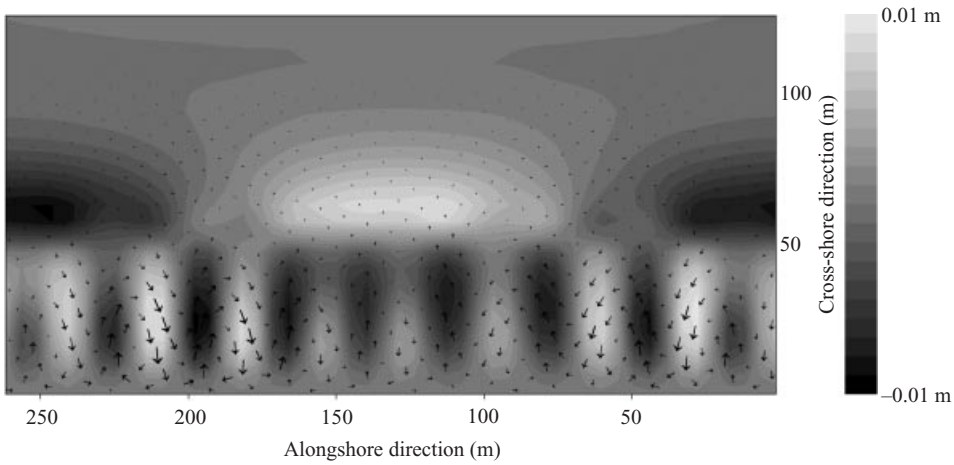

FIGURE 7. Formation and development of a mixed bar pattern. Shoals and troughs are represented by light and dark colours respectively. The coastline is at the bottom.

morphology and the circulation are in qualitative agreement with the linear instability mode found in Falqués *et al.* (2000). However, a finite amplitude can be determined. For the simulation presented in figure 5 it is around 0.2 m (in other cases a growth up to 0.5 m can be simulated) and, as shown in figure 6 the growth rate of the pattern is slower but the trend is very similar to that observed for the transverse bar pattern (figure 4). The intensity of the circulation associated with the bar is about $0.35\,\mathrm{m\,s^{-1}}$. In fact, although sediment is being moved and bedforms begin to appear, bed perturbations do not grow significantly during the first 2 h. Again for the crescentic bar pattern the final spacing is proportional to the width of the surf zone. In general agreement with the field observations (see for example the observations reported in Bown & Inman 1971), it is between 4 and 5 times the width of the surf zone.

4.5. *Transverse versus crescentic bars*

A question arises as to why two simulations with an essentially similar parameterization result in such different patterns. First, it is important to underline that the transition between one pattern and the other is difficult to detect accurately since it corresponds to complicated topographies where the dominant pattern is difficult to discern. Figure 7 shows the results of a simulation run with the same parameterization as figure 1 apart from $N = 0.0075$. It provides a clear example of a mixed topography with transverse and crescentic bars developing non-uniformly (note the smaller amplitude of the bars 'shaded' by the presence of a crescentic shoal). The possibility that such complicated topography might arise should not be considered as a shortcoming of the model as many observations report similar patterns in nature (see for example Goldsmith *et al.* 1982). Nevertheless, it is possible to find some trends in the parameter space that favour either CB or TB formation.

The numerical simulations show that small values of the morphodynamic diffusion γ_m result in the dominance of transverse bars. Higher values lead to mixed patterns, to crescentic bars or to stability. The momentum diffusion coefficient, N, plays a similar role, low values leading to TB, higher values leading to CB. With respect to wave height, the trend is that small H favours CB while with larger waves TB dominate. On the other hand, the analysis related to the effect of the friction coefficient, c_d, clearly

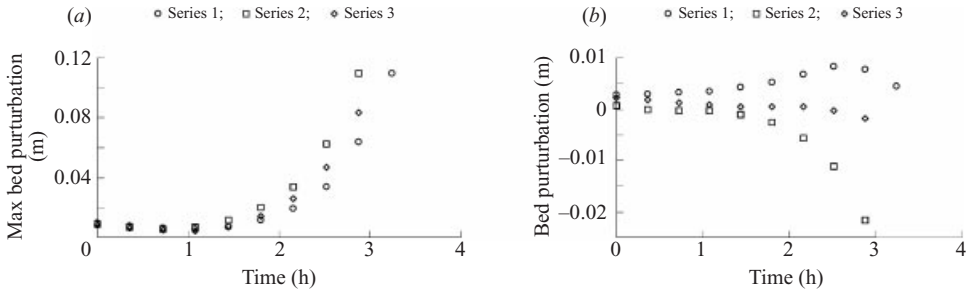

FIGURE 8. Growth rates for three simulations differing only in the seed used for the generation of the initial topography. (*a*) Maximum bed perturbation, and (*b*) perturbation at a fixed location inside the surf zone.

indicates that, maintaining all the other parameters constant, small (large) values of friction result in the appearance of the crescentic (transverse) sand bar pattern.

Another aspect of interest, especially as we are dealing with nonlinear simulations, concerns the importance of the initial perturbation imposed on the sea bed elevations. In order to test the importance of the initial conditions and determine how much they can affect final configurations, simulations have been run using the same parameters and changing only the seed used when producing the initial sea bed perturbation. Results for three simulations (series 1, 2 and 3) all leading to the appearance of a transverse bar pattern are shown in figure 9. It is evident that growth rates of the maximum amplitudes are only slightly affected by such changes (figure 8*a*). On the other hand, when analysing the growth rate at single locations inside the surf zone, significant differences (in magnitude and even sign) can be observed (figure 8*b*). Overall, the three simulations all result in a transverse bar pattern with the same spacing although the locations of troughs and shoals differ (figure 9). The effect of the initial bed perturbation amplitude on the process of pattern formation has also been analysed and, as expected, the only difference detected between the different simulations is in the growth rates, with bigger initial amplitudes resulting in a faster growth of the features. The physical mechanism responsible for the generation of the bars and the physical interpretation of the dominance of TB or CB will be discussed in § 5.

5. Physical mechanisms

5.1. *Bottom evolution equation*

Even though a predictive modelling of sand bar formation and evolution needs to solve the full system of the governing equations (2.1), (2.2) and (2.3), a simple bottom evolution equation derived only from water and sediment mass conservation, i.e. (2.1) and (2.3), is very useful in understanding the physical mechanisms responsible for the growth of the bedforms.

Since the hydrodynamics respond much faster than the morphodynamics, the common quasi-steady approximation, e.g. that the flow adjusts instantaneously to the topographic changes, will be considered in this section. Thus, the time derivative drops out of the mass conservation equation (2.3) so that

$$\nabla \cdot \boldsymbol{v} = -\frac{1}{D}\boldsymbol{v} \cdot \nabla D. \tag{5.1}$$

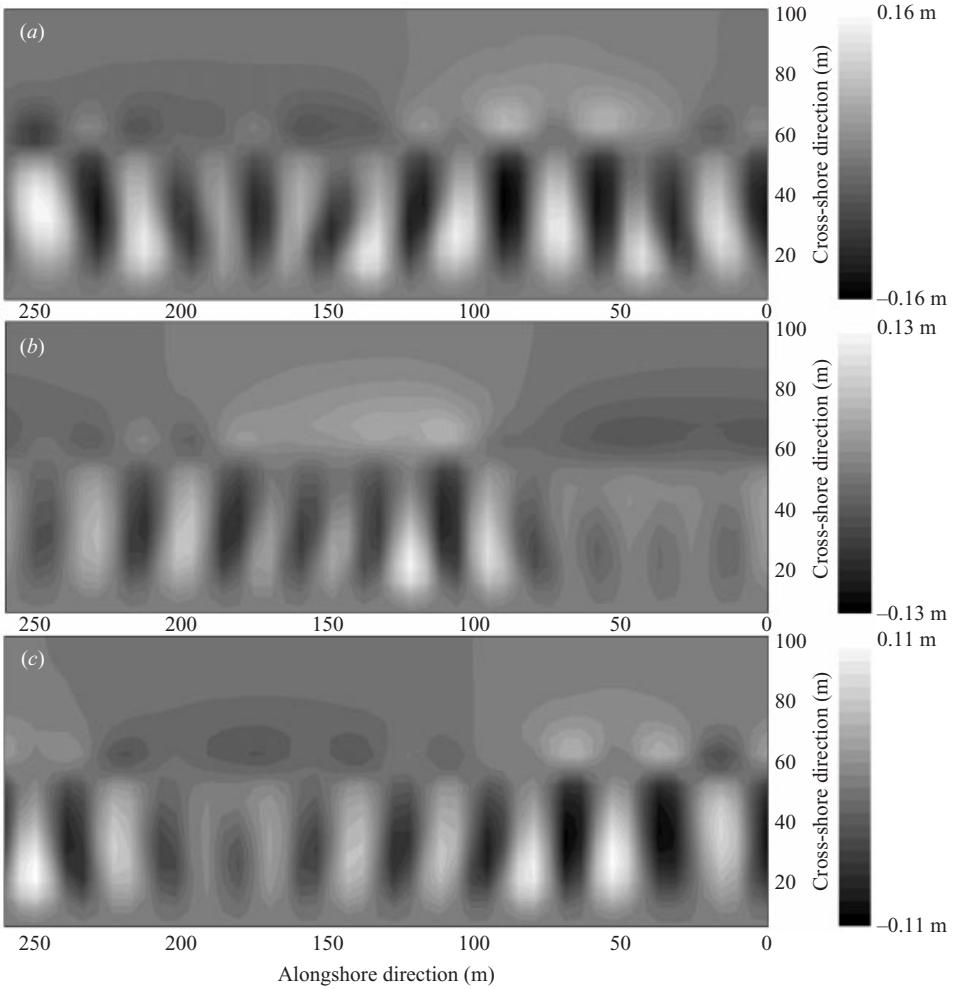

FIGURE 9. Final configurations obtained for three simulations differing only in the seed used for the generation of the initial topography. Shoals and troughs are represented by light and dark colours respectively. The coastline is at the bottom of each plot.

In this section, the sediment transport parameterization (2.10) will be extended to allow for a nonlinear dependence on the current

$$\boldsymbol{q} = \alpha(u_0) v^{m-1} \boldsymbol{v}, \tag{5.2}$$

where $v = |\boldsymbol{v}|$, $\alpha(u_0)$ is the wave stirring coefficient and $u_0(x, y)$ is the wave orbital velocity. On the other hand, the morphological diffusion has been disregarded in this section since it produces just a damping of the bedforms and it is not essential for the generation mechanism.

The bottom evolution equation follows from the sediment conservation equation (2.1) and the expansion

$$\nabla \cdot \boldsymbol{q} = v^{m-1} \boldsymbol{v} \cdot \nabla \alpha + \alpha v^{m-1} \nabla \cdot \boldsymbol{v} + \alpha \boldsymbol{v} \cdot \nabla (v^{m-1}).$$

Taking the identities

$$\frac{\partial}{\partial x_i}(v^{m-1}) = (m-1)v^{m-3}v_j\frac{\partial v_j}{\partial x_i},$$

$$\boldsymbol{v}\cdot\nabla\alpha - \frac{\alpha}{D}\boldsymbol{v}\cdot\nabla D = \alpha\boldsymbol{v}\cdot\nabla\ln\left(\frac{\alpha}{D}\right),$$

and (5.1) into account, the equation

$$\frac{\partial z_b}{\partial t} = -\alpha v^{m-1}\boldsymbol{v}\cdot\nabla\ln\left(\frac{\alpha}{D}\right) - (m-1)\alpha v^{m-2}a_T \tag{5.3}$$

is finally obtained, where $a_T = \boldsymbol{v}\cdot\nabla\boldsymbol{v}\cdot\boldsymbol{v}/v$ is the tangential component of the advective acceleration of the fluid.

Equation (5.3) gives the morphological effect of any mean flow pattern, $\boldsymbol{v}(x, y, t)$, according to the sediment transport parameterization (5.2) and will be hereinafter referred as the BEE (bottom evolution equation). According to it, accretion will occur at the locations where the right-hand side is positive and erosion where it is negative. The physical meaning of the second term on the right is simple: a deceleration of the flow ($a_T < 0$) produces a decrease of sediment carrying capacity and hence accretion, since the sediment flux decreases downstream. This term appears only if the sediment transport is nonlinear in the mean current, $m > 1$. The first term produces accretion whenever the current opposes the gradient in the α/D function. This can be understood by decomposing it into two terms proportional to $-\boldsymbol{v}\cdot\nabla\alpha$ and to $\boldsymbol{v}\cdot\nabla D$ respectively. Since the sediment carrying capacity of the flow is proportional to α, a current running in the direction of the gradient of α (i.e. $-\boldsymbol{v}\cdot\nabla\alpha < 0$) will produce a downstream increase of sediment flux and, therefore, erosion will occur. Finally, a current running into deeper water (i.e. $\boldsymbol{v}\cdot\nabla D > 0$) should slow down due to mass conservation. This causes a convergence of the sediment flux since it is proportional to a power of the flow velocity and, thereby, accretion will take place. It is important to realize that the BEE gives the morphological evolution only if the flow pattern is known and this requires solution of the full system (5.3), (2.2) and (2.3). However, since the flow associated with crescentic and transverse bars obtained by numerical simulation in § 4 is in agreement with physical intuition, the BEE will provide a quite simple physical explanation of the generation of both patterns.

5.2. *Bed–surf instability mechanism*

The possibility of a positive feedback between the growing rhythmic topography and the circulation induced by breaking waves over this topography will be analysed in this section. The analysis is similar to that presented in Falqués *et al.* (2000) but it is now extended to include wave refraction.

In case of suspended-load transport and in accordance with the discussion in § 2.2.2, $\alpha(x)/D(x)$ is expected to increase from the shoreline up to a maximum close to the breaking line and to decrease seaward of this maximum. This is due to the fact that the stirring of the waves on the sediment is maximum at the breaking line. Since the simulations presented here have been carried out with the sediment transport parameterization (2.10), i.e. $m = 1$, let us concentrate on the effect of the first term on the right-hand side of the BEE which is the only non-vanishing one. Some comments on the effect of the second term will be given in § 5.3.

According to the BEE, a shoal in the surf zone will grow if the current runs on it against the gradient in α/D, that is, shoreward. Therefore, a positive feedback between the rhythmic topography and the circulation will occur if the current is onshore over

the shoals and offshore over the pools. To investigate now whether this is the case, let us look at the cross-shore momentum input from the breaking waves:

$$F_x = -\frac{1}{\rho D}\left(\frac{\partial S_{xx}}{\partial x} + \frac{\partial S_{xy}}{\partial y}\right)$$
$$= -\frac{1}{8}g\gamma_b^2\left(\frac{1}{D}\frac{\partial}{\partial x}\left[\left(\frac{1}{2} + (\cos\varphi)^2\right)D^2\right] - \frac{D}{2}\frac{\partial}{\partial y}(\sin 2\varphi) - \frac{\partial D}{\partial y}\sin 2\varphi\right), \quad (5.4)$$

where (2.4), (2.5) and (2.6) together with $k_x = -k\cos\varphi$, $k_y = k\sin\varphi$ have been taken into account. Also, the phase and the group celerity are considered to be approximately equal, $c \simeq c_g$. Let us assume that the perturbation of the mean free surface is relatively small compared to the bed perturbation, so that the perturbation in water depth is given approximately by $-h(x, y, t) = -(z_b - z_b^0)$. In view of the numerical simulations and of the analysis of the 'flow over topography problem' in Falqués *et al.* (2000) this is reasonable. For bedforms with relatively small amplitude the wave angle is not too big, so that $1 + 2(\cos\varphi)^2) \simeq 3$ and, also, the term $-(\partial D/\partial y)\sin 2\varphi = (\partial h/\partial y)\sin 2\varphi$ can be neglected (second order in the perturbations). Thus, the perturbation in the cross-shore momentum input is

$$\delta F_x = \frac{1}{8}g\gamma_b^2\left(3\frac{\partial h}{\partial x} + \frac{D_0}{2}\frac{\partial}{\partial y}(\sin 2\varphi)\right). \quad (5.5)$$

With respect to the basic state, the first term provides an onshore force on the water column at the seaward portion of the shoal and offshore at the shoreward portion. Thus, the resulting flow direction is not clear from the present analysis. Furthermore, as also shown by Sancho *et al.* (1995), even though the wave radiation stress is the primary cause for the currents, the actual circulation is also affected by the mean surface slopes. However, this term (in combination with pressure gradients) was already considered in the linear stability analysis of Falqués *et al.* (2000) and it was seen to be capable of producing a net onshore current for certain shapes of the shoal (those corresponding to the linearly unstable modes). The second term, related to wave refraction, was not considered in that paper and it produces a net onshore force on the water over the entire shoal. Indeed, consider a shoal extending symmetrically over both sides of the y-axis (see figure 2). Due to wave refraction, $\varphi > 0$ for $y < 0$ and $\varphi < 0$ for $y > 0$ so that $\partial/\partial y(\sin 2\varphi) < 0$ on average over the shoal. This terms appears thanks to the inflow of wave cross-shore momentum through the lateral flanks of the shoal produced by refraction. Cross-shore wave momentum is focused over the shoals where it is dissipated as waves break. The magnitude of this term increases onshore since $|\varphi|$ increases onshore as the wave rays bend towards shallower water as they propagate onshore. Therefore, the combined effect of both terms is expected to produce a net onshore current over the shoals and just the opposite over the pools in between the shoals. Thus, a positive feedback is expected between morphology and hydrodynamics. The reason why this mechanism can generate two patterns that are so different will be explained in the next section.

5.3. *Crescentic and transverse bars*

To understand the occurrence of both patterns, let us assume that the corresponding shoals in the surf zone have a cross-shore extent of $\sim l_x$ and an alongshore spacing of λ. Let Δh be the scale for the bed level perturbation and $\Delta\varphi$ the scale of the angle between the refracted wavevector and the shore normal. Then, the corresponding

scaling of the first and the second terms F_1, F_2 in (5.5) gives

$$\frac{F_1}{F_2} \sim \frac{3}{2}\frac{\Delta h}{d\Delta\varphi}\frac{\lambda}{l_x}, \tag{5.6}$$

with d being the scale for the water depth. The bottom perturbation h and the wave angle φ both grow in time proportionally to each other at the initial formation. Therefore, the magnitude of this ratio can be evaluated from their typical values for moderate-amplitude bedforms: $\Delta h \sim 0.1$ m and $\Delta\varphi \sim 0.1$ rad. Assuming a water depth scale of $d \sim 1$ m the scaling

$$\frac{F_1}{F_2} \sim \frac{3}{2}\frac{\lambda}{l_x} \tag{5.7}$$

is obtained. Two limits can now be considered:

(*a*) *Long-wavelength limit* ($\lambda \gg l_x$). In this case F_2 is negligible, that is, wave refraction is negligible and the emerging pattern is the crescentic bar pattern predicted by the linear stability analysis of Falqués *et al.* (2000) where only F_1 was accounted for. Since the current, with respect to the basic state, tends to be offshore at the shoreward part of the surf zone shoals, the shoals cannot grow towards the coastline and are therefore located close to the breaking line. The onshore current over the surf zone shoals crosses the breaking line and therefore creates pools seaward of the breaking line because the gradient in α/D has an opposite direction in the shoaling region. Conversely, and again with respect to the basic state, the offshore current over the surf zone pools produces shoals seaward of the breaking line. In this way, the typical mirroring effect of alternating shoals and pools is created.

(*b*) *Short-wavelength limit* ($\lambda \sim l_x$). In this case, both F_1 and F_2 are comparable and refraction is important. Now, because of F_2, the current is onshore over the entire shoal even if the shoal extends almost up to the coastline. This fact, in combination with the small alongshore spacing between the shoals, gives finger-like bedforms elongated in the cross-shore direction, that is, transverse bars. This explanation is in agreement with the results of the numerical simulations and the suggestions of Niederoda & Tanner (1970) that wave refraction is essential for TB generation. The shape of the TB is in contrast with that of CB since the latter have rounded shoals because the shoals are widely spaced and with small cross-shore extent.

Thus, CB and TB are just the long-wavelength and the short-wavelength limits of the same instability mechanism. In the case of TB the circulation is more intense because the net hydrodynamic force is onshore over the entire bar whereas for CB there is an offshore component over part of the surf zone shoals. This is clearly seen in the numerical simulations and, as a result, the growth of TB is faster and TB dominate in the absence of dissipative damping. However, since TB essentially have shorter wavelengths than CB, they imply stronger gradients in the topography and in the hydrodynamics. Therefore, they are more damped than CB by an increasing diffusivity both morphologically and hydrodynamically (momentum). This provides the explanation of why TB dominate in the case of low γ_m and N while CB tend to dominate for high values. The role of wave height becomes evident if the non-dimensional morphological diffusion is considered (the same scaling used in Falqués *et al.* 2000 has been adopted here):

$$\Gamma = \frac{\gamma_m}{\alpha_m\sqrt{gH}}. \tag{5.8}$$

It is then clear that large waves result in a smaller non-dimensional diffusivity if γ_m and α_m are kept constant and lead therefore to TB.

In the set of input parameters of the model, the wave height, H, and α_m and γ_m are independent. In nature however the wave stirring, α_m, and the morphological diffusivity, γ_m, clearly depend on the wave height. Even though the relationships are dependent on the parameterization used, an impression of the trends can be obtained by considering the Bailard formula for suspended load, (2.11). In this case, the expression

$$\Gamma = \frac{\varepsilon_s \gamma_b}{4} \frac{\sqrt{gH}}{w} \tag{5.9}$$

is obtained, where w is the sediment grain fall velocity and the shallow-water approximation for the orbital velocity, $u_0 = 0.5H\sqrt{g/D}$ has been used. This expression reveals that when the dependence of γ_m upon H is considered, the influence of H on the transition TB/CB dominance is reversed with respect to the raw output of the model, where γ_m and H are handled as if independent. It now becomes apparent that for very high waves and very fine sand (small w) there is stability: no alongshore rhythmicity appears. Moderate waves and less fine sediment lead to crescentic bars and smaller waves and relatively coarse sand lead to transverse bars. This is consistent with the sequence of wave-dominated beach changes described by Short (1999): 'dissipative', 'rhythmic bar and beach', 'transverse bar and beach'. On the other hand, a necessary condition for the growth of the instabilities is an α/D function increasing seaward in the surf zone, a condition not met for bedload sediment transport. Therefore, for even smaller waves and coarser sediment, suspended load would not occur and a second region with no large-scale rhythmic features would exist. This would correspond to the reflective beach stage of Short (1999). The simulations presented in §4 were performed for the case of a sediment transport linear in the current, e.g. $m = 1$, in which case the second term on the right-hand side of the BEE vanishes. For an m exponent larger than 1, the first term has just a different proportionality factor so that the mechanism just described is expected to work in a similar way. We should only look for the additional effect of the second term on the right-hand side. This is easily seen to reinforce the generation of the crescentic bar since the associated circulation has deceleration ($a_T < 0$) over the shoals and acceleration ($a_T > 0$) over the pools. Thus, the mechanism for the crescentic bar generation does not depend on the particular choice of the exponent m in the sediment transport, a result that agrees with the findings by Werner & Fink (1993). In the case of TB the onshore current decelerates where the bars attach to the shoreline and accelerates at the seaward end of the bars. Therefore, if $m > 1$, the a_T term in the BEE would enhance the shoreline attachment (possible cusp formation) and would counteract the term related to $\nabla(\alpha/D)$ at the seaward end, thereby controlling the length of the bars.

6. Discussion

The primary limitation of the present study is its inability to reach saturation to an equilibrium amplitude because of the critical angle for wave refraction. This problem does not prevent the development of realistic scales for features (a few decimetres). Several effects that have been neglected in the present approach should be considered for future research on the final saturated stages of the bars. First, it should be stressed that the present sediment flux parameterization is linear in the mean-current velocity. Such an assumption is strictly valid only for small-amplitude features (with the wave

orbital velocity exceeding the mean current) although it has been argued that the nonlinear terms do not change the essense of the patterns. This is confirmed by the fact that the finite-amplitude patterns of flow and morphology resulting from the numerical simulations favourably compare with field observations. However, the nonlinear terms can have an influence on the final shape and amplitude. The same applies to the influence of perturbations on the wave stirring, which has proven to be of no importance for the growth to realistic amplitudes. Wave refraction due to the currents may also be important as a saturation mechanism and should be incorporated.

Another simplification is that shoaling has been neglected based on the assumption that wave breaking is the main driving force of surf zone circulation. This has been carefully checked and the main conclusion is the following. For nearly normal incidence, the main hydrodynamic forcing comes from

$$\frac{\partial S_{xx}}{\partial x} \simeq \frac{3}{2}\frac{\partial E}{\partial x}. \tag{6.1}$$

In the surf zone, the wave energy density is proportional to D^2 while in the shoaling zone it is roughly proportional to $D^{-1/2}$ as it can be seen from $c_g \simeq c \simeq \sqrt{gD}$. Thus, a given perturbation in water depth will produce a perturbation in energy four times larger if it is located in the surf zone than if it is located in the shoaling zone. The same applies for $\partial S_{xx}/\partial x$. Now, since the perturbations in $\partial S_{xx}/\partial x$ are proportional to the perturbations in $\partial D/\partial x$, the relevant question is whether the perturbations in water depth are larger in the surf zone or in the shoaling zone. For the transverse bar pattern, the perturbations out of the surf zone (if any) are very small. Therefore, the effect of shoaling can clearly be neglected. For the crescentic bars, the perturbations in water depth in the shoaling zone are about two times smaller than the perturbations in the surf zone at the initial stages of the pattern formation. Therefore, the forcing because of shoaling would be about 1/8 of the forcing due to breaking so that it can be safely neglected for the initial formation. During the final stages of the simulations, the water depth perturbations outside the surf zone become comparable, in general, to the perturbations inside the surf zone. However, despite the differences in the ratio between 'inner amplitude' and 'outer amplitude' all these solutions present the same spatial pattern in the flow and in the morphology. This indicates that even though the shoaling could be significant for crescentic bars of large amplitude, it does not affect the initial development of the features nor their essential characteristics.

A potential important limitation is the simplified description of sediment transport based on the departure from equilibrium due only to the net currents while the perturbations in wave-driven transport are neglected. Although this assumption has been shown to be reasonable, it deserves future attention.

Field observations of crescentic patterns are usually related to the presence of an initially uniform longshore bar and the pattern is superimposed on it to give what is generally called a 'crescentic bar'. Work is in progress to evaluate if the mechanism proposed herein also operates over this kind of topography. That study, the first step towards specific comparisons with field observations, clearly involves changes in the sediment transport parameterization with, for example, a stirring related to the water depth. Such an effort has already been undertaken and preliminary results (Coco *et al.* 2002) seem to indicate the appearance of rhythmic features also over an initially barred profile (uniform in the alongshore direction).

The present study has been limited to waves approaching normally to the coast in deep water. Nevertheless, the existing linear stability analyses for oblique wave

incidence (see, for instance, Deigaard *et al.* 1999 and Ribas, Falqués & Montoto 2000) suggest that rhythmic patterns can self-organize in this case also and due to similar mechanisms.

An important aspect when dealing with the formation and development of morphological features is the time scale of growth of the patterns and, more generally, of the different processes operating in the nearshore region. In the parameterization proposed here, α_m measures the intensity of the wave stirring and can be evaluated according to any particular sediment transport parameterization. In the scaling presented in Falqués *et al.* (2000) the morphological time scale was proportional to α_m^{-1} (equation 18 in that paper). This implies that α_m has two effects: (i) to determine the ratio ϵ between the hydrodynamical and the morphological time scales and (ii) to give the dimensional growth time of the bars. It was found that for a realistic range of values, the variation of ϵ produced hardly any effect on the non-dimensional instability analysis. Thus, the effect of changing α_m is simply to change the growth time of the bars. In the numerical simulations presented in § 4, a default value of $\alpha_m = 0.01$ m has been used. According to field data presented by Peters & Dette (1999) for waves of $H \simeq 0.7$ and 1.2 m, and grain size about 0.3 mm, a reasonable estimate for the maximum sediment concentration at the bed in the surf zone in such conditions can be some $10\,\mathrm{g\,l^{-1}}$, i.e. 0.004 (volume of sand per total volume). Taking into account the fact that the vertical distribution was relatively uniform or smoothly decreasing upwards and the water depth was about 1 m, a reasonable estimate for the depth-integrated concentration would be $\alpha_m \simeq 0.002$ m. This would mean that the use of $\alpha_m = 0.01$ m would develop morphological features about a factor 5 too fast. Therefore, the growth times obtained in § 4 must be multiplied by a factor of about 5 to obtain realistic times. The use of a value larger than that estimated from field observations was motivated by computing concerns: fewer time steps are needed to simulate morphological evolution over a given total real time. This can be safely done as long as the morphological time scale remains much larger than the hydrodynamical time scale ($\epsilon \ll 1$).

Finally, it is important to underline that the instability mechanism can operate only if the infragravity wave energy fraction is not too large. Otherwise, the wave stirring function $\alpha(x)$ would show a nearly uniform profile across the surf zone. In such a case, both earlier studies (Falqués *et al.* 2000) and the present research indicate that instabilities do not develop. This is in agreement with the observations by Holman & Sallenger (1993), where: 'The alongshore bar became crescentic soon after a storm when the infragravity band variance was observed to decline' and also with the observation that high-energy, planar beaches (i.e. Scripps, Torrey Pines), which tend to have a lot of infragravity energy, do not tend to have crescentic or transverse patterns.

7. Conclusions

It has been shown that large-scale patterns in the nearshore region can arise from small randomly placed irregularities of the sea bed. Such perturbations of the sea bottom grow and self-organize to a regular spacing due to a positive feedback between flow and morphology without the need of any low-frequency hydrodynamic external forcing like edge waves. The positive feedback between flow and morphology is based on three essential ingredients: (i) a wave stirring function increasing seaward faster than water depth up to the breaking line (its actual dependence does not affect the results), (ii) a depth-limited wave height in the surf zone, and (iii) the topographic refraction of the waves. These three ingredients are likely to be present in the surf

zone if sediment transport takes place mainly in suspension. Under such assumptions, more (less) dissipation of momentum occurs over a shoal (trough) with respect to the alongshore uniform equilibrium. Thus, a larger (smaller) onshore hydrodynamic force occurs at the shoals (troughs) and a net onshore (offshore) current is created at the shoals (troughs). This is supported by many observations (see for example Sonu 1972, 1973; Wright & Short 1984). The assumption of a seaward-increasing wave stirring then ensures that a positive (negative) budget of sediment occurs at the shoals (pools) and positive feedback is thus created.

The model can exhibit a complex temporal behaviour with a variety of patterns evolving, merging and changing length-scale, but the dynamics are clearly driven by the competition between two main patterns that, like features observed in nature, have been called crescentic bars (CB) and transverse bars (TB). The former are a double series of shoals and pools alternating on both sides of the mean breaking line showing a mirroring effect. The latter are finger-like elongated bars perpendicular to the shore. The emergence of these two very different patterns from the same 'bed–surf' coupling has been related to the fact that wave refraction increases in importance with decreasing alongshore spacing of the features. Thus, for closely spaced shoals (compared to their cross-shore extent) refraction becomes very important and permits their growth across the whole surf zone, resulting in elongated shore-normal bars. For widely spaced shoals, refraction is negligible and the circulation coupled to them allows only growth close to the breaking line, resulting in crescentic bars. In the absence of damping, TB dominate due to the stronger circulation driven by wave refraction. However, due to their closer spacing, they are associated with strong gradients both in the morphology and in the hydrodynamics. As a result they are more inhibited by increasing diffusivity of both the morphology and the hydrodynamics. Therefore, for low diffusion TB dominate while for relatively large diffusion CB dominate. For very high diffusivity neither of the patterns grows and the initial alongshore uniform morphology is stable. The conditions for the occurrence of either TB or CB, or for the absence of large-scale rhythmic features in the model can also be interpreted in terms of wave height and sediment grain size by using the Bailard (1981) parameterization of sediment transport (see (5.3)). In this case, the predictions of the model compare well with the beach state sequence described by Short (1999): the sequence of stability–CB–TB–stability when going from high to small waves and from fine to coarse sand. Physical explanations for the precise spacing of the bedforms are more difficult to formulate but our numerical results show that the alongshore wavelength of both patterns scales with the width of the surf zone, being 4–5 times larger for CB and about half for TB.

In the past, Bowen & Inman (1971) have explained CB as the morphological response to an external forcing by edge waves. Alternative explanations based on linear morphodynamic instabilities have been given by Vittori *et al.* (1999), Deigaard *et al.* (1999) and Falqués *et al.* (2000). However, the present work is the first in which finite-amplitude modelling of CB has been presented. The present findings are even more important in the case of TB, since no model, either hydrodynamically driven or based on self-organization, has previously provided an explanation for these elongated shore-normal bars that are frequently observed in nature. In particular, the linear stability analysis of Falqués *et al.* (2000) did not predict the formation of TB since wave refraction was not included. Similarly, the hydrodynamically driven model of Holman & Bowen (1982) predicted a variety of different complex patterns but not this type of transverse bar. Furthermore, the earlier suggestion of Niederoda & Tanner 1970, based on field and laboratory experiments, that topographic wave refraction was the primary cause of TB has now been clearly confirmed. The present

explanation based on normal wave incidence processes is also in agreement with the recent finding of Konicki & Holman (2000) that TB appear not to be correlated with longshore currents.

Due to the lack of detailed measurements, comparisons with field observations can, at present, only be made on a qualitative basis. The shape and spacing of the patterns resemble those described by several authors (Davis & Fox 1972; Goldsmith *et al.* 1982; Konicki & Holman 2000; Niederoda & Tanner 1970; Short 1999) but only a limited number of studies have given an indication of the prevailing hydrodynamic conditions (Konicki & Holman 2000; Niederoda & Tanner 1970). Observed and modelled feature amplitudes are in agreement though it should be stressed that such comparisons cannot be conclusive due to the difficulty of reaching a steady state in the numerical runs. Specific field measurements are needed in order to test the present findings and in particular to determine the flow patterns over developing features, the form of the cross-shore variation of the wave stirring and morphological diffusion functions. Further field observations are also required to test the model predictions of the range of conditions under which the patterns emerge.

Funding from the European Union under contracts MAS3 CT97-0081 (SASME project) and EVK3-2000-22014 (HUMOR project) are gratefully acknowledged. Miquel Caballeria and Albert Falqués are also indebted to the Spanish DGESIC under contract PB98-0929. Giovanni Coco was supported by US Navy-Office of Naval Research Scholar Award (N00014-97-10154), the Andrew W. Mellon Foundation and the University of Plymouth. The authors would like to thank B. T. Werner, R. T. Guza and the three anonymous reviewers for their constructive comments.

Appendix A. Quasi-steady morphodynamic processes

The morphological evolution follows from the sediment budget in a water column, that is, the amount of the sediment that goes in through the lateral walls of a control volume that either accretes at the bottom or enters into suspension in the water column. This can be written as

$$-\nabla \cdot \boldsymbol{q} = (1-p)\frac{\partial z_b}{\partial t} + \frac{\partial C}{\partial t} \tag{A 1}$$

(Caballeria 2000) where p stands for porosity, $1-p$ is the volumetric rate between dry sediment and wet sediment, $z = z_b(x, y, t)$ is the level of the sea bed, $\boldsymbol{q}$ is the horizontal sediment flux vector (volume per length and time units) and C is the vertically integrated sediment concentration (volume per area unit).

For quasi-steady morphodynamic processes (a definition is provided below), this equation can be reduced to (2.1). Let us consider a horizontal length scale given by the horizontal gradients in sediment flux, $[L_h]$, and a vertical length scale, $[L_v]$. If the scale for the volumetric three-dimensional sediment concentration is $[c]$, the scale for two-dimensional vertically integrated concentration will be $[c][L_v]$ and the scale for the sediment flux, $\boldsymbol{q}$, will be $[c][V][L_v]$ where $[V]$ is the scale for the water flow velocity. Thus, let us consider the scaling

$$(x, y) = (x', y')[L_h], \tag{A 2}$$

$$z_b = z_b'[L_v], \tag{A 3}$$

$$C = C'[c][L_v], \tag{A 4}$$

$$q = q'[c][V][L_v]. \tag{A 5}$$

With respect to time, three scales can be defined as follows: the morphological time, $[T_m]$, which is the time scale of the bottom evolution; the scale of the variations in the suspended sediment concentration, $[T_c]$; and the hydrodynamic time, $[T_h] = [L_h]/[V]$. In the situation of interest for the present work, $[L_h] \sim 50\,\mathrm{m}$ and $[V] \sim 0.5\,\mathrm{m\,s^{-1}}$ so the hydrodynamic time scale (wind/swell-wave-averaged hydrodynamics) is of order $T_h \sim 10^2$ s. Two time variables may then be defined:

$$t = t'[T_m] = t''[T_c], \tag{A 6}$$

so that the scaled bottom evolution equation (A 1) reads

$$(1-p)\frac{\partial z_b'}{\partial t'} + [c]\,\frac{[T_m]\,[V]}{[L_h]}\,\nabla' \cdot \boldsymbol{q}' + [c]\frac{[T_m]}{[T_c]}\frac{\partial C'}{\partial t''} = 0. \tag{A 7}$$

The *storage term* $\partial C/\partial t$ can be neglected provided that

$$[c]\,\frac{[T_m]}{[T_c]} \ll [c]\frac{[T_m][V]}{[L_h]}, \tag{A 8}$$

that is,

$$[T_c] \gg \frac{[L_h]}{[V]} = [T_h], \tag{A 9}$$

which means that the relevant changes in sediment concentration must be much slower than the hydrodynamics. The class of processes fulfilling this condition and described by the simplified equation

$$(1-p)\frac{\partial z_b}{\partial t} + \nabla \cdot \boldsymbol{q} = 0 \tag{A 10}$$

can be called *quasi-steady morphodynamic processes*. In this case, the morphological time scale can easily be estimated. Because of the definition of the scales, the first term in the bottom evolution equation (A 7) is of order one. This means that the coefficient in front of the divergence of the sediment flux must be of order one too. This determines the morphological time scale

$$[T_m] = \frac{[L_h]}{[V][c]} \gg \frac{[L_h]}{[V]} = [T_h]. \tag{A 11}$$

The inequality states that the morphological time scale is much larger than the hydrodynamic one and follows from the experimental fact that the volumetric sediment concentration is typically not larger than $[c] \sim 0.01$.

The simplification cannot be made if the relevant changes in sediment concentration occur at the same time as the hydrodynamics, $[T_c] \sim [T_h] \sim 10^2$ s. For instance, the storage term cannot be neglected if the potential morphological effect of infragravity waves is included.

Appendix B. Sediment transport formulation

The physical grounds for the sediment transport parameterization, (2.10), used in this paper will be presented here. Prior to introducing sediment transport it is convenient to define some hydrodynamic concepts. Regular waves of period T and height H are assumed so that mean quantities are defined by:

$$\langle f \rangle = \frac{1}{T}\int_0^T f(t)\,\mathrm{d}t.$$

If D_0 is the depth under wave troughs at a given position, the *current below troughs* is defined by

$$\boldsymbol{U} = \frac{1}{D_0} \int_{z_b}^{z_b+D_0} \langle \boldsymbol{u} \rangle \, \mathrm{d}z,$$

where z is the vertical coordinate, $z = z_b$ is the bed level and $\boldsymbol{u}$ is the instantaneous fluid velocity at a given position. This is different from the total depth-integrated current $\boldsymbol{v}$ of the shallow-water formulation, (2.2) and (2.3), which is given by

$$\boldsymbol{v} = \frac{1}{\bar{D}} \left\langle \int_{z_b}^{z_s} \boldsymbol{u} \mathrm{d}z \right\rangle,$$

where $z = z_s$ is the instantaneous sea level and $\bar{D} = \langle z_s - z_b \rangle$. We will refer to it as the *total current*. The total water volume flux at a given position can then be written as

$$\bar{D}\boldsymbol{v} = D_0 \boldsymbol{U} + \boldsymbol{m}, \tag{B 1}$$

where $\boldsymbol{m}$ is the water volume flux due to the waves which is located between troughs and crests.

Let us now turn to sediment transport. It is reasonable to expand the total sediment flux (bedload and suspended load) into three contributions: transport driven by the currents, transport driven by the waves and downslope transport driven by gravity:

$$\boldsymbol{q} = \boldsymbol{q}_c + \boldsymbol{q}_w + \boldsymbol{q}_g. \tag{B 2}$$

By 'transport driven by the waves' we mean the transport due to wave asymmetry, wave skewness, etc. The 'transport driven by gravity' is the downslope contribution caused by gravity. This approach may be supported for instance by the widely adopted formulation given by Bailard (1981).

Our first assumption on sediment transport is that the current-driven transport consists of two contributions, one proportional to the water volume flux below troughs and the other proportional to the water volume flux above troughs:

$$\boldsymbol{q}_c = c_1 D_0 \boldsymbol{U} + c_2 \boldsymbol{m}, \tag{B 3}$$

where c_1 and c_2 are the effective depth-averaged sediment concentrations below and above troughs respectively; c_2 is expected to be much smaller than c_1. In general, the concentrations c_1, c_2 can depend on the current $\boldsymbol{U}$ so that $\boldsymbol{q}_c$ will not be linear in $\boldsymbol{U}$. However, in the case where the net currents are smaller than the wave orbital velocity, u_0, the concentrations c_1, c_2 will depend mainly on u_0 and can be considered as independent of the current (see, for instance, Bailard's 1981 formulation for $|\boldsymbol{U}| \ll u_0$). The bedload transport contribution is assumed to be included in the effective concentration below troughs, c_1. Notice that, consistent with the shallow-water approximation used in the present work, the possible contributions due to the stratification of both the flow and the sediment concentration are disregarded in (B 3). This expression corresponds in fact to a double-layer model. By using (B 1), (B 3) can be rewritten as

$$\boldsymbol{q}_c = c_1 D_0 \boldsymbol{v} - (c_1 - c_2)\, \boldsymbol{m}. \tag{B 4}$$

Let us consider the steady alongshore-uniform equilibrium state where there is neither mean water flux, $\boldsymbol{v} = 0$, nor mean sediment flux, $\boldsymbol{q} = 0$. On using the former condition the latter reads

$$\boldsymbol{q}_w^0 + \boldsymbol{q}_g^0 - (c_1^0 - c_2^0)\, \boldsymbol{m}^0 = 0. \tag{B 5}$$

Notice that in equilibrium, even though the total current vanishes, $\boldsymbol{v} = 0$, the current below troughs, $\boldsymbol{U}$, is not zero due to the undertow. Let us now examine the perturbed state where alongshore non-uniformity develops and $\boldsymbol{v} \neq 0, \boldsymbol{q} \neq 0$. Subtraction of (B 5) from (B 2), and taking account of (B 4) yields

$$\boldsymbol{q} = c_1 \bar{D} \boldsymbol{v} + \boldsymbol{q}'_w + \boldsymbol{q}'_g - (c'_1 - c'_2)\, \boldsymbol{m} - (c^0_1 - c^0_2)\, \boldsymbol{m}', \tag{B 6}$$

where the primes mean perturbed quantities, that is, $c'_1 = c_1 - c^0_1$, $\boldsymbol{m}' = \boldsymbol{m} - \boldsymbol{m}^0$ and so on. Then, our second assumption is that the perturbations in the wave-driven sediment transport and in the transport due to the water flux above troughs are negligible compared to the sediment transport due to the total current:

$$|\boldsymbol{q}'_w|, \quad |(c^0_1 - c^0_2)\boldsymbol{m}'|, \quad |(c'_1 - c'_2)\, \boldsymbol{m}| \ll |c_1 \bar{D} \boldsymbol{v}|. \tag{B 7}$$

Finally we adopt the common expression (Bailard 1981)

$$\boldsymbol{q}_g = -\gamma \nabla z_b$$

for the gravity-driven transport, where γ depends on the wave orbital velocity. With all these assumptions, our sediment transport equation can be finally written as

$$\boldsymbol{q} = \alpha \boldsymbol{v} - \gamma \nabla z'_b, \tag{B 8}$$

where $z'_b = z_b - z^0_b$ and $\alpha = c_1 \bar{D}$.

Let us check the order of magnitude of the quantities involved in inequality (B 7). We will refer to a typical situation with

$$\bar{D} \sim 2\,\mathrm{m}, \quad H \sim 1\,\mathrm{m}, \quad v \sim 0.5\,\mathrm{m\,s^{-1}}, \quad u_0 \sim 1\,\mathrm{m\,s^{-1}}, \quad c_1 \sim 0.001, \tag{B 9}$$

in which the order of magnitude of the current-driven sediment transport will be $|c_1 \bar{D} \boldsymbol{v}| \sim 10^{-3}\,\mathrm{m^2\,s^{-1}}$. We will assume moderate-amplitude topographic perturbations not larger that about 10% the mean water depth, $\bar{D}$.

An estimate of the wave-driven sediment transport $\boldsymbol{q}_w$ can be made by considering the alongshore-uniform equilibrium. In this case, $\boldsymbol{q}_w$ is balanced by the transport driven by gravity and undertow. The three contributions are thus of the same order of magnitude (see Plant *et al.* 2000) so that an evaluation of $\boldsymbol{q}_g$ provides a reasonable estimate of the magnitude of $\boldsymbol{q}_w$. We can compute the coefficient γ in $\boldsymbol{q}_g$ by means of the Bailard (1981) parameterization. By adapting equation (11) in that paper to volume of sediment instead of weight we obtain

$$\gamma = \frac{c_d}{gs} \frac{\varepsilon_b}{(\tan \phi_c)^2} + \left(\frac{\varepsilon_s}{w_s} \right)^2 u_0^2 u_0^3, \tag{B 10}$$

where $\epsilon_b \simeq 0.1$, $\epsilon_s \simeq 0.02$, $c_d \sim 0.01$, $\tan \phi_c \simeq 1$. The relative density of the sediment is $s \simeq 2.6$ and we can consider, for instance, a fall celerity of the grains $w_s \sim 0.05\,\mathrm{m\,s^{-1}}$. With all these figures, we obtain $\gamma \sim 2 \times 10^{-4}\,\mathrm{m^2\,s^{-1}}$. To obtain an upper bound we can assume a very steep slope of $|\nabla z_b| \sim 0.1$ and we finally arrive at $|\boldsymbol{q}_w| \sim |\boldsymbol{q}_g| \sim 2 \times 10^{-5}\,\mathrm{m^2\,s^{-1}}$. This estimate is not in disagreement with experimental data reported by Peters, Newe & Oumeraci (2001) who found $|\boldsymbol{q}_w| \sim 10^{-4}\,\mathrm{m^2\,s^{-1}}$ for storm conditions (much stronger than the 'typical' situation considered here). It is reasonable to assume that the perturbation of this wave-driven transport for moderate-amplitude topographic perturbations is not larger than $\boldsymbol{q}_w$ itself. Thus, $\boldsymbol{q}'_w$ is expected to be at most one or two orders of magnitude smaller than the current-driven transport.

The water volume flux driven by the waves can be computed as

$$|\boldsymbol{m}| = \frac{E}{\rho c} \sim \frac{1}{8}\sqrt{\frac{g}{\bar{D}}}H^2, \tag{B 11}$$

which gives $m = |\boldsymbol{m}| \sim 0.3\,\mathrm{m^2\,s^{-1}}$. If we assume that the perturbations in c_1, c_2 are not larger than 10% of c_1 itself, it immediately follows that $|(c_1' - c_2')\,\boldsymbol{m}|$ is not larger than $0.3 \times 10^{-4}\,\mathrm{m^2\,s^{-1}}$.

If we insert the saturated surf zone hypothesis, $H = \gamma_b \bar{D}$, into (B 11) we find the relationship $m'/m = 1.5\bar{D}'/\bar{D}$ between the relative variations. From this,

$$m' \sim 1.5 \times 0.1 \times 0.3\,\mathrm{m^2\,s^{-1}} \sim 0.05\,\mathrm{m^2\,s^{-1}}$$

and, since $c_1^0 \sim 0.001$, it is found that $|(c_1^0 - c_2^0)\boldsymbol{m}'| \sim 0.5 \times 10^{-4}\,\mathrm{m^2\,s^{-1}}$. Therefore, it is sensible to neglect the three terms on the left in (B 7) with respect to the current-driven sediment transport.

REFERENCES

Antsyferov, S. M. & Kos'yan, R. 1990 Study of suspended sediment distribution in the coastal zone. *Coastal Engng* **14**, 147–172.

Bailard, J. A. 1981 An energetics total load sediment transport model for a plane sloping beach. *J. Geophys. Res.* **86** (C11), 10938–10954.

Battjes, J. A. 1975 A note on modeling of turbulence in the surf zone. In *Proc. Symp. Modeling Tech., San Francisco*, pp. 1050–1061. ASCE.

Battjes, J. A. 1988 Surf zone dynamics. *Annu. Rev. Fluid Mech.* **20**, 257–293.

Blondeaux, P. 1990 Sand ripples under sea waves. Part 1. Ripple formation. *J. Fluid Mech.* **218**, 1–17.

Bowen, A. J. & Inman, D. L. 1971 Edge waves and crescentic bars. *J. Geophys. Res.* **76**, 8662–8671.

Caballeria, M. 2000 Self-organization in the nearshore: shear waves, transverse and crescentic bars. PhD thesis, Univ. Politècnica de Catalunya, Barcelona.

Calvete, D., Falqués, A., De Swart, H. E. & Walgreen, M. 2001 Modelling the formation of shoreface-connected ridges on storm-dominated inner shelves. *J. Fluid Mech.* **441**, 169–193.

Christensen, E., Deigaard, R. & Fredsoe, J. 1995 Sea bed stability on a long straight coast. In *Proc. 24th Intl Conf. Coastal Engng*, pp. 1865–1879. ASCE.

Coco, G., Caballeria, M., Falqués, A. & Huntley, D. H. 2002 Crescentic bars and nearshore self-organization processes. In *Proc. 28th Intl Conf. Coastal Engng*. ASCE (accepted).

Coco, G., Huntley, D. A. & O'Hare, T. J. 2000 Investigation of a self-organisation model for beach cusp formation and development. *J. Geophys. Res.* **105** (C9), 21991–22002.

Davis, R. A. & Fox, W. 1972 Coastal processes and nearshore sand bars *J. Sediment. Petrol.* **42**, 401–412.

Dean, R. G. 1991 Equilibrium beach profiles: characteristics and application. *J. Coastal Res.* **7**, 53–84.

Deigaard, R., Droonen, N., Fredsoe, J., Jensen, J. H. & Jorgesen, M. 1999 A morphological stability analysis for a long straight barred coast. *Coastal Engng* **36**, 171–195.

Falqués, A. 1989 Formación de topografía rítmica en el delta del ebro. *Revista de Geofísica* **45**, 143–156.

Falqués, A., Coco, G. & Huntley, D. A. 2000 A mechanism for the generation of wave-driven rhythmic patterns in the surf zone. *J. Geophys. Res.* **105** (C10), 24071–24088.

Falqués, A., Montoto, A. & Iranzo, V. 1996 Bed-flow instability of the longshore current. *Continental Shelf Res.* **16**, 1927–1964.

Goldsmith, V., Bowman, D. & Kiley, K. 1982 Sequential stage development of crescentic bars: Hahoterim beach, southeastern mediterranean. *J. Sediment. Petrol.* **52**, 233–249.

Hino, M. 1975 Theory formation of rip-current and cuspidal forms. In *Proc. 14th Intl Conf. Coastal Engng*, pp. 901–919. ASCE.

Holland, K. T. & Holman, R. A. 1996 Field observations of beach cusps and swash motions. *Mar. Geol.* **134**, 77–93.

Holman, R. A. & Bowen, A. J. 1982 Bars, bumps, and holes: models for the generation of complex beach topography. *J. Geophys. Res.* **87**, 457–468.

Holman, R. A. & Sallenger, A. H. 1993 Sand bar generation: a discussion of the duck experiment series. *J. Coastal Res.* **15**, 76–92.

Horikawa, K. 1988 *Nearshore Dynamics and Coastal Processes*. University of Tokyo Press.

Hulscher, S. J. M. H., De Swart, H. E. & De Vriend, H. J. 1993 The generation of offshore tidal sand banks and sand waves. *Continental Shelf Res.* **13**, 1183–1204.

Inman, D. L. & Guza, R. T. 1982 The origin of swash cusps on beaches. *Mar. Geol.* **49**, 133–148.

Konicki, K. M. & Holman, R. A. 2000 The statistics and kinematics of transverse bars on an open coast. *Mar. Geol.* **169**, 69–101.

Lippmann, T. C. & Holman, R. A. 1990 The spatial and temporal variability of sand bar morphology *J. Geophys. Res.* **95** (C7), 11575–11590.

Longuet-Higgins, M. S. 1970 Longshore currents generated by obliquely incident sea waves, 1. *J. Geophys. Res.* **75**, 6778–6789.

Masselink, G. & Pattiaratchi, C. B. 1998 Morphological evolution of beach cusp morphology and associated swash circulation patterns. *Mar. Geol.* **146**, 93–113.

Mei, C. C. 1989 *The Applied Dynamics of Ocean Surface Waves*. World Scientific.

Niederoda, A. W. & Tanner, W. F. 1970 Preliminary study on transverse bars. *Mar. Geol.* **9**, 41–62.

Peters, K. & Dette, H. H. 1999 Sediment suspension in the surf zone. In *Coastal Sediments'99* (ed. N. C. Kraus & W. G. McDougal), pp. 195–208. ASCE.

Peters, K., Newe, J. & Oumeraci, H. 2001 Characterization of sediment transport. In *Coastal Dynamics'01* (ed. H. Hanson & M. Larson), pp. 293–302. ASCE.

Plant, N. G., Ruessink, B. G. & Wijnberg, K. M. 2000 Morphologic properties derived from a simple cross-shore sediment transport model. *J. Geophys. Res.* **106** (C1), 945–958.

Ribas, F., Falqués, A. & Montoto, A. 2000 Normal mode analysis of the surf zone morphodynamics. In *Coastal Engineering 2000* (ed. B. Edge), pp. 3229–3242. ASCE.

van Rijn, L. C. 1993 *Principles of Sediment Transport in Rivers, Estuaries and Coastal Seas*. Aqua Publications, Amsterdam, The Netherlands.

Russell, R. J. & Mcintire, W. G. 1965 Beach cusps. *Geol. Soc. Am. Bull.* **76**, 307–320.

Sancho, F. E., Svendsen, I. A., Dongeren, A. R. V. & Putrevu, U. 1995 Longshore nonuniformities of nearshore currents. In *Coastal Dynamics'95*, pp. 425–436. ASCE.

Short, A. D. 1999 *Handbook of Beach and Shoreface Morphodynamics* (ed. A. D. Short). Wiley.

Sonu, C. 1972 Field observation of nearshore circulation and meandering currents. *J. Geophys. Res.* **77** (18), 3232–3247.

Sonu, C. 1973 Three-dimensional beach changes. *J. Geology* **81**, 42–64.

Vittori, G., De Swart, H. E. & Blondeaux, P. 1999 Crescentic bedforms in the nearshore region. *J. Fluid Mech.* **381**, 271–303.

Werner, B. T. & Fink, T. M. 1993 Beach cusps as self-organised patterns. *Science* **260**, 968–971.

Wright, L. D. & Short, A. D. 1984 Morphodynamic variability of surf zones and beaches: a synthesis. *Mar. Geol.* **56**, 93–118.